

# Analytic wave model of Stark deceleration dynamics

Koos Gubbels, Gerard Meijer, and Bretislav Friedrich

Fritz-Haber-Institut der Max-Planck-Gesellschaft, Faradayweg 4-6, D-14195 Berlin, Germany

(Received 2 February 2006; published 12 June 2006)

Stark deceleration relies on time-dependent inhomogeneous electric fields which repetitively exert a decelerating force on polar molecules. Fourier analysis reveals that such fields, generated by an array of field stages, consist of a superposition of partial waves with well-defined phase velocities. Molecules whose velocities come close to the phase velocity of a given wave get a ride from that wave. For a square-wave temporal dependence of the Stark field, the phase velocities of the waves are found to be odd-fraction multiples of a fundamental phase velocity  $\lambda/\tau$ , with  $\lambda$  and  $\tau$  the spatial and temporal periods of the field. Here we study explicitly the dynamics due to any of the waves as well as due to their mutual perturbations. We first solve the equations of motion for the case of single-wave interactions and exploit their isomorphism with those for the biased pendulum. Next we analyze the perturbations of the single-wave dynamics by other waves and find that these have no net effect on the phase stability of the acceleration or deceleration process. Finally, we find that a packet of molecules can also ride a wave which results from an interference of adjacent waves. In this case, small phase stability areas form around phase velocities that are even-fraction multiples of the fundamental velocity. A detailed comparison with classical trajectory simulations and with experiment demonstrates that the analytic “wave model” encompasses all the longitudinal physics encountered in a Stark decelerator.

DOI: 10.1103/PhysRevA.73.063406

PACS number(s): 32.60.+i, 32.80.Pj, 45.50.-j

## I. INTRODUCTION

Achieving an ever better control over both the internal and external degrees of freedom of gas-phase molecules has been a prominent goal of molecular physics over the last decades. Molecular beams, both continuous and pulsed, have been widely used to produce large densities of molecules in selected quantum states. In these beams, the longitudinal temperature of the molecules is typically 1 K, and the mean velocity of the beam can be varied between about 300 and 3000 m/s by adjusting the temperature of the source or by using different carrier gases. Control over the spatial orientation or alignment of molecules in a beam has been achieved by actively manipulating the rotation of the molecules using electrostatic or magnetic multipole fields as well as with the help of laser radiation. The application of inhomogeneous fields has enabled control over the transverse motion of the oriented or aligned molecules, and thus their state selection [1–3].

The control over the longitudinal motion of molecules in a molecular beam has been greatly enhanced as well. In 1999, it was first demonstrated that an array of time-varying, inhomogeneous electric fields can slow down a beam of polar molecules [4]. This so-called Stark decelerator for neutral polar molecules is the equivalent of a linear accelerator (LINAC) for charged particles. In a Stark decelerator, the quantum-state specific force that acts on a polar molecule subject to an electric field is exploited. This force is rather weak, typically some eight to ten orders of magnitude weaker than the force that would act on the molecular ion in the same electric field. This force nevertheless suffices to provide complete control over the motion of polar molecules, using techniques akin to those used for the control of charged particles. This has been explicitly demonstrated by the construction of two different types of linear decelerators [4,5], a buncher [6], a mirror [7], two different types of traps [8,9]

and a storage ring [10] for neutral polar molecules.

A crucial feature of the Stark decelerator is its phase stability. Phase stability, which is at the core of synchrotron-like charged-particle accelerators as well [11], enables to hold together a packet of neutral molecules throughout the Stark-deceleration process. Phase-stable operation of a Stark decelerator, viewed as trapping of neutral molecules in a traveling potential well, was first explicitly demonstrated in experiments on metastable CO [12]. In that work, as well as in later publications on the deceleration of various isotopomers of ammonia, the one-dimensional (1D) equation of motion for molecules that undergo phase-stable transport was stated [12–14]. In order to obtain the longitudinal equation of motion, the Stark energy (potential energy) of the molecules was expressed as a function of position along the longitudinal decelerator axis, and the change in Stark energy per deceleration stage was evaluated. As this treatment did not yield *a priori* an expression for the force on the molecules as a function of time, assumptions about the time dependence of the force were made in order to arrive, in an intuitive way, at the equation of motion. The validity of these assumptions was checked against trajectory calculations, and it had been concluded that this equation of motion indeed describes correctly the physics of the phase-stable motion in a Stark decelerator [12–14]. Nevertheless, a mathematically rigorous derivation of the equation of motion and an in-depth analysis of the complex dynamics in a Stark decelerator was still wanting.

A description of the (longitudinal) force acting on the molecules as a function of both their position in the decelerator and as a function of time could be obtained by expressing the spatial and temporal dependence of the electric fields in the decelerator in terms of a Fourier series [15]. This description, in which the force has been expressed as an infinite sum of stationary and counter-propagating waves, contained all the correct physics, but it was not directly evident how to connect this description to the trajectory calcu-

lations or to the actual experiments. In particular, it was not clear why, in discussing phase stability, it is allowed to only consider the interaction of the molecules with one of the infinitely many waves. It was not clear either where the experimentally observed first- and second-order resonances in the decelerator—which have a straightforward interpretation in the intuitive model [16]—come from the Fourier-series description.

In this paper, we give a detailed description of the *longitudinal* motion of molecules in a Stark decelerator (or accelerator). This description is based on the Fourier analysis of the force that acts on the molecules as a function of position and time [15]. The motion of the molecules in phase space due to any of the interacting waves, as well as due to their mutual perturbations, is analyzed. A detailed comparison with trajectory calculations and experiment has shown that the “wave model” presented here holds up to all the scrutiny applied, and provides a complete and accurate description of the longitudinal dynamics of polar molecules in a Stark decelerator.

Thus our treatment here is restricted to the motion along the molecular beam axis. In more recent work, the coupling between the transverse and the longitudinal motion was included, and the transverse stability in a Stark decelerator was discussed as well [17].

## II. FOURIER REPRESENTATION OF THE ELECTRIC FIELD IN A STARK ACCELERATOR OR DECELERATOR

Figure 1 shows a prototypical switchable field array suitable for accelerating or decelerating polar molecules. The electric fields are generated by *field stages* (rod-electrode pairs, cylindrical electrodes, or other) longitudinally separated by a distance  $\lambda/2$ . In the array, every other field stage is energized and every other grounded. Which field stages are energized and which are grounded determines one of two possible *field configurations* of the array. Figure 1(a) shows, for the case of four field stages, the electric fields that are generated by the two field configurations. The magnitudes of the electric fields that pertain to the upper and lower field configuration are shown by the red and blue curves and will be referred to as the red,  $\varepsilon_r$ , and blue,  $\varepsilon_b$ , field, respectively. Also shown is the longitudinal coordinate  $z$ . A given field stage is energized or grounded during a time  $\tau/2$ , after which the fields are *switched*, i.e., the field stages that were energized become grounded and the field stages that were grounded become energized. Figure 1(b) shows the *alternation* between the red and blue fields as a function of time,  $t$ . An energized field stage becomes grounded or vice versa during a transient time,  $\Delta\tau$ . For  $\Delta\tau \ll \tau$ , the temporal alternation between the red and blue fields is *square-wave like*.

We will now represent the spatial and temporal dependence of the *net field*, which results from the switching between the static red and blue fields, by a Fourier series.

We will begin by Fourier expanding the spatial dependence of the red field, which is produced by field stages at positions  $z = (\frac{3}{4} + m)\lambda$ , with  $m = 0, 1, 2, 3, \dots$ , see Fig. 1(a). The strength of the red field is given by

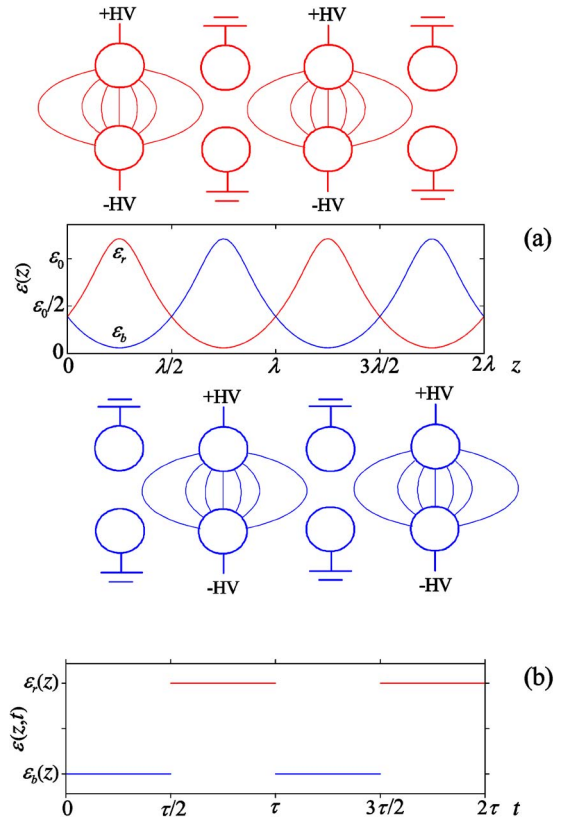


FIG. 1. (Color online) A prototypical switchable field array that generates fields suited for accelerating or decelerating polar molecules. The field stages are longitudinally separated by a distance  $\lambda/2$ . Every other field stage is energized and every other grounded. There are two possible field configurations. (a) Electric fields generated by the two field configurations (for the case of four field stages). The electric fields that pertain to the upper and lower field configurations are shown by the red and blue curves and are referred to here as the red,  $\varepsilon_r$ , and blue,  $\varepsilon_b$ , fields, respectively. Also shown is the longitudinal coordinate  $z$ ; (b) Alternation between the red and blue fields as a function of time,  $t$ . A given field stage is energized or grounded during a time  $\tau/2$ , after which the fields are switched, i.e., the field stages that were energized become grounded and vice versa. An energized field stage becomes grounded or vice versa during a transient time,  $\Delta\tau$ . The figure pertains to the case of guiding, for which the period  $\tau$  is constant. The case of a varying period is shown in Fig. 2.

$$\varepsilon_r(z) = \frac{1}{2}\varepsilon_0 + \sum_{m=1}^{\infty} \varepsilon_m \cos(m\varphi), \quad (1)$$

where  $\varepsilon_m$  are the spatial Fourier coefficients and

$$\varphi \equiv 2\pi z/\lambda - \pi/2. \quad (2)$$

The blue field is produced by field stages at positions  $z = (\frac{3}{4} + m)\lambda$ , see Fig. 1(a), and so is obtained from the red field by shifting it by  $\lambda/2$ , i.e.

$$\varepsilon_b(z) = \varepsilon_r\left(z - \frac{\lambda}{2}\right) = \frac{1}{2}\varepsilon_0 + \sum_{m=1}^{\infty} (-1)^m \varepsilon_m \cos(m\varphi). \quad (3)$$

Taking  $\Delta\tau = 0$ , the net field,  $\varepsilon(z, t)$ , is given by

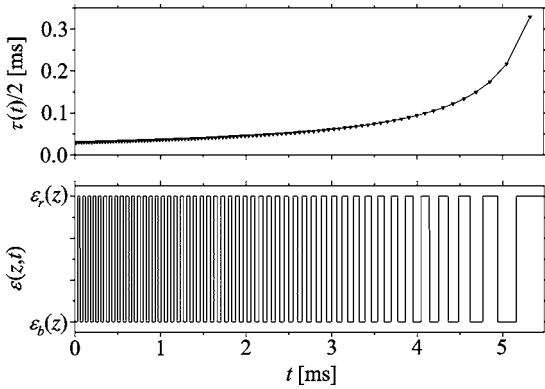


FIG. 2. The time dependence of the field pertaining to the case of deceleration, for which the period  $\tau$  is a function of time,  $\tau = \tau(t)$ . The case of a constant period is shown in Fig. 1. The timing sequence, generated by Eq. (33), is suitable for decelerating OH radicals on the  $(+, 1, 1)$  wave with  $\phi_s = 53^\circ$  from an initial velocity of 370 m/s to a final velocity of 25 m/s in the decelerator presented in Refs. [17,16]. The upper panel shows the corresponding dependence of the switching half period,  $\tau(t)/2$ . The points mark the time difference between two subsequent switching times. See Sec. IV C.

$$\begin{aligned} \varepsilon(z,t) &= \varepsilon_b(z) \quad \text{for } 0 < t < \pi/2, \\ \varepsilon(z,t) &= \varepsilon_r(z) \quad \text{for } \pi/2 < t < \tau, \end{aligned} \quad (4)$$

see Fig. 1(b).

In order to derive the Fourier representation of the net field, we will expand Eq. (4) in terms of a temporal Fourier series. By invoking the “well-known” result for a temporal square wave [18], the net field can be written as

$$\begin{aligned} \varepsilon(z,t) &= \frac{1}{2}[\varepsilon_b(z) + \varepsilon_r(z)] + \frac{1}{2}[\varepsilon_b(z) - \varepsilon_r(z)] \\ &\times \sum_{\ell \text{ odd}}^{\infty} \frac{4}{\pi\ell} \sin(\ell\theta), \end{aligned} \quad (5)$$

where  $\theta$  is the temporal phase such that

$$\dot{\theta}(t) = \omega(t) = \frac{2\pi}{\tau(t)} \quad (6)$$

with  $\omega$  the angular frequency. While Fig. 1(b) shows a time dependence of the field with a constant period  $\tau$  (which corresponds to the so-called *guiding*, see below), Fig. 2 shows a time sequence with a varying period  $\tau = \tau(t)$  (one which corresponds to *deceleration*). In either case, the square wave rises and falls when the temporal phase becomes equal to an integer multiple of  $\pi$ .

Substitution into Eq. (5) from Eqs. (1)–(3) yields

$$\begin{aligned} \varepsilon(z,t) &= \frac{1}{2}\varepsilon_0 + \sum_{p \text{ even}}^{\infty} (-1)^{1/2p}\varepsilon_p \cos(pkz) \\ &+ \sum_{n \text{ odd}}^{\infty} \sum_{\ell \text{ odd}}^{\infty} \frac{4}{\pi\ell}(-1)^{1/2(n+1)}\varepsilon_n \sin(nkz)\sin(\ell\theta) \\ &= \frac{1}{2}\varepsilon_0 + \sum_{p \text{ even}}^{\infty} (-1)^{1/2p}\varepsilon_p \cos(pkz) \\ &+ \sum_{n \text{ odd}}^{\infty} \sum_{\ell \text{ odd}}^{\infty} \frac{2}{n\ell}(-1)^{1/2(n+1)} \\ &\times \varepsilon_n (\cos \phi_{+,n,\ell} - \cos \phi_{-,n,\ell}), \end{aligned} \quad (7)$$

where we made use of the identity  $\sin \alpha \sin \beta = \frac{1}{2}[\cos(\alpha - \beta) - \cos(\alpha + \beta)]$ , defined the spatial frequency (wave vector)

$$k \equiv 2\pi/\lambda \quad (8)$$

and introduced the *phase*

$$\phi_{\pm,n,\ell} \equiv nkz \mp \ell\theta. \quad (9)$$

Note that  $p, n, \ell$  are all positive integers.

Equation (7) reveals that the net field consists of a superposition of *stationary* and of *pair-wise counter-propagating partial waves*. The propagating waves move with *well-defined phase velocities*

$$\begin{aligned} V_{\pm,n,\ell} &\equiv -\frac{(\partial \phi_{\pm,n,\ell}/\partial t)_z}{(\partial \phi_{\pm,n,\ell}/\partial z)_t} = \pm \frac{\ell \dot{\theta}(t)}{n k} = \pm \frac{\ell \omega(t)}{n k} = \pm \frac{\ell}{n} \frac{\lambda}{\tau(t)} \\ &\equiv \pm \frac{\ell}{n} V(t) \end{aligned} \quad (10)$$

from left to right (+ sign) and from right to left (− sign). The second line of Eq. (10) defines the *fundamental phase velocity*,  $V(t)$ , which is determined solely by the spatial and temporal periods  $\lambda$  and  $\tau(t)$ .

The path taken here in deriving Eq. (7) is a shortcut of the route used to derive the same equation in our previous work [15]. The time dependence of the temporal period or frequency is here emphasized right from the outset.

Note that the spatial Fourier coefficients  $\varepsilon_m$  along with the square-wave time dependence fully characterize the net field. While the temporal Fourier coefficients fall only as  $\ell^{-1}$ , the spatial ones fall off roughly exponentially with  $m$ , i.e.

$$\varepsilon_m \propto \exp[-\xi m], \quad (11)$$

where  $\xi$  is a decay parameter which depends on the geometry of the field array. Hence we can expect waves with small  $n$  and larger  $\ell$  to dominate; as we will see in Sec. V, waves with  $n \leq 5$  and  $\ell \leq 21$  account for all the dynamics observed so far.

### III. POTENTIAL AND FORCE

A molecule with a space-fixed electric dipole moment  $\langle \mu \rangle = \langle \mu(\varepsilon) \rangle$  subject to field (7) has a Stark energy

$$W(z,t) = -\langle \mu(\varepsilon) \rangle \varepsilon(z,t). \quad (12)$$

In what follows, we will consider molecular states whose space-fixed electric dipole moment is independent of the electric field strength; this is the case when the field-molecule interaction is governed by the first-order Stark effect. Molecular states whose space-fixed electric dipole moment  $\langle \mu \rangle$  is parallel ( $\langle \mu \rangle > 0$ ) or antiparallel ( $\langle \mu \rangle < 0$ ) to the electric field strength are referred to as *high* or *low-field seeking states*, respectively. Whereas the eigenenergy of high-field seekers decreases with increasing field strength, it increases for the low-field seekers. As a result, in an inhomogeneous electric field, such as  $\varepsilon(z,t)$ , high-field seekers seek regions of maximum, and low-field seekers seek regions of minimum field strength where their eigenenergy is minimal. In the net field (7), the Stark energy becomes

$$\begin{aligned} W(z,t) = & \frac{1}{2} W_0 + \sum_{p \text{ even}}^{\infty} (-1)^{1/2p} W_p \cos(pkz) \\ & + \sum_{n \text{ odd}}^{\infty} \sum_{\ell \text{ odd}}^{\infty} \frac{2}{\pi\ell} (-1)^{1/2(n+1)} W_n (\cos \phi_{+,n,\ell} \\ & - \cos \phi_{-,n,\ell}) \end{aligned} \quad (13)$$

with

$$W_i = -\langle \mu \rangle \varepsilon_i \quad i = 1, 2, 3, \dots \quad (14)$$

We note that in the case of nonlinear Stark effect [19], Eq. (13) can still be used to represent the Stark energy, although Eq. (14) is no longer valid. In order to obtain the correct Fourier coefficients  $W_i$ , we need to first numerically calculate the Stark energy of a molecule in the two electric-field configurations  $\varepsilon_r(z)$  and  $\varepsilon_b(z)$ . Subsequently, we can Fourier expand the Stark energy, just as we expanded the electric field, and extract the  $W_i$  coefficients, which leaves Eq. (13) intact [20].

Since the Stark energy plays the role of a potential for the motion of the molecules, the force,  $F(z,t)$ , that the field exerts on a molecule of mass  $M$  is given by

$$\begin{aligned} F(z,t) = & -\frac{dW(z,t)}{dz} = \sum_{p \text{ even}} MA_p \sin(pkz) \\ & + \sum_{n \text{ odd}} \sum_{\ell \text{ odd}} MA_{n,\ell} (\sin \phi_{+,n,\ell} - \sin \phi_{-,n,\ell}), \end{aligned} \quad (15)$$

where

$$\begin{aligned} A_p & \equiv (-1)^{1/2p} \frac{pk}{M} W_p, \\ A_{n,\ell} & \equiv (-1)^{1/2(n+1)} \frac{2nk}{\pi\ell M} W_n. \end{aligned} \quad (16)$$

Thus we see that a molecule subject to force (15) is acted upon by an infinite multitude of stationary as well as propagating and counter-propagating waves. However, as we will see in Sec. IV, only a single wave governs the molecule-field interaction. Which wave it is determined by the difference between the wave's phase velocity and the velocity of the

molecule: only a wave whose initial phase velocity comes close to the initial velocity of the molecule can become paramount. In order to find out how close this needs to be, we must do the dynamics.

#### IV. DYNAMICS OF THE INTERACTION OF MOLECULES WITH A SINGLE WAVE

In this section we will examine the dynamics of the interaction of a bunch of molecules with a single wave. After developing a formalism for describing such an interaction and discussing its dynamics, we will be able to show why, to an excellent approximation, the effect of all the other waves can be neglected. In Sec. V we will consider the full-fledged dynamics and evaluate explicitly the perturbing effects due to other waves. We will also tackle the (marginal) effects due to interfering waves which interact jointly with a bunch of molecules.

##### A. Force exerted by an arbitrary wave

As we can glean from Eqs. (7), (13), and (15), an arbitrary propagating wave can be labeled by a pair of *odd* integers,  $n$  and  $\ell$ , and by its propagation direction (+ for left to right or - for right to left), i.e., by  $(\pm, n, \ell)$ . Since the molecules move from left to right by convention, in what follows we will consider waves moving from left to right. Thus such an otherwise arbitrary wave travels from left to right with a phase velocity

$$V_{n,\ell} \equiv V_{+,n,\ell} = \frac{\ell \dot{\theta}}{n k}, \quad (17)$$

cf. Eq. (10), and exerts a force on a molecule given by

$$F_{n,\ell}(z,t) = M A_{n,\ell} \sin \phi_{n,\ell} \quad (18)$$

with the phase

$$\phi_{n,\ell} \equiv \phi_{+,n,\ell} = nkz - \ell \theta. \quad (19)$$

The corresponding acceleration then becomes

$$a_{n,\ell} \equiv \ddot{z}_{n,\ell} = \frac{F_{n,\ell}(z,t)}{M} = A_{n,\ell} \sin \phi_{n,\ell}. \quad (20)$$

##### B. Synchronous molecule and its velocity

A key concept in tackling the molecule-wave interaction is that of a *synchronous molecule*. This is defined as the molecule which maintains a *constant (synchronous) phase*

$$\phi_s \equiv (\phi_{n,\ell})_s = nkz_s - \ell \theta = \text{const.} \quad (21)$$

with respect to a *given wave*  $(n, \ell)$  throughout the acceleration or deceleration process—no matter what, see Fig. 3.

It should be noted that the definition of the synchronous phase given here is slightly different from the definition that has been used in earlier descriptions of phase stability in a Stark decelerator [12–14,16]. In these earlier studies the synchronous phase was defined in terms of the position of the synchronous molecule relative to the electrodes, and this po-

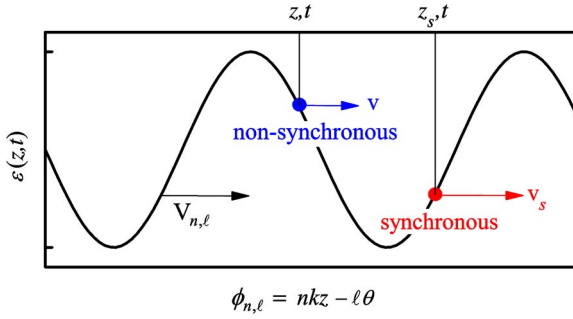


FIG. 3. (Color online) A synchronous and a nonsynchronous molecule subjected to the field  $\varepsilon(z,t)$  of a  $(+, n, \ell)$  wave moving at a phase velocity  $V_{n,\ell}$  (all motion is from left to right). The change of the velocity,  $v_s$ , of a synchronous molecule is such that its phase  $\phi_s$  with respect to the traveling field remains constant. This is the case when  $v_s = V_{n,\ell}$ . The velocity,  $v$ , of a nonsynchronous molecule and its phase,  $\phi$ , change with time. Also shown are the spatial coordinates of the synchronous and nonsynchronous molecule,  $z_s$  and  $z$ , respectively.

sition was required to be the same every time the electric fields were switched from one configuration to the other. Although this definition takes the full spatial dependence of the Stark interaction into account, it only specifies the synchronous phase at the moment when the fields are switched. In the case when the spatial and temporal dependence of the Stark interaction is governed by a single wave  $(n, \ell)$ , the definitions are equivalent.

From Eq. (18) it immediately follows that the synchronous molecule is acted upon by a *constant force*

$$(F_{n,\ell})_s = MA_{n,\ell} \sin \phi_s \quad (22)$$

and thus has a *constant acceleration*

$$(a_{n,\ell})_s = A_{n,\ell} \sin \phi_s \equiv a_s. \quad (23)$$

From Eq. (23) we see that the acceleration/deceleration rate can be *tuned by tuning the synchronous phase*. As follows from Eq. (21), at  $t=0$ , when the fields are switched for the first time, the synchronous phase is simply

$$\phi_s(z_s, t=0) = nkz_s. \quad (24)$$

Therefore, the synchronous phase can be tuned by launching the *switching sequence* (or *burst*) when the synchronous molecule has the desirable longitudinal coordinate  $z_s$ . The subsequent switching times between the two field configurations can always be chosen such that the synchronous molecule will keep the same phase.

With a tunable acceleration or deceleration, the initial velocity of the synchronous molecule can be increased or decreased to any value

$$v_s(t) = v_s(t=0) + a_s t. \quad (25)$$

### C. Phase velocity, temporal phase, and switching sequence

In order to keep the phase of the synchronous molecule constant during acceleration or deceleration, the phase veloc-

ity of the wave that interacts with the molecule needs to be varied. This is done by applying a *variable* switching sequence to the field array as the molecule progresses through it. In other words, the temporal frequency or period of the applied field is made time dependent,  $\omega = \omega(t)$  or  $\tau = \tau(t)$ . As a result, the phase velocity becomes also time dependent, cf. Eq. (10). In this paragraph we will show that the phase velocity of the wave is always equal to the synchronous velocity of the molecule, as one would expect. Furthermore, we will evaluate the temporal phase and hence the timing sequence needed to *keep* a molecule synchronous.

From the definition of the synchronous phase, Eq. (21), we obtain

$$\dot{\phi}_s = 0 = nk\dot{z}_s - \ell \dot{\theta} \quad (26)$$

from which it follows that

$$\dot{z}_s \equiv v_s = \frac{\ell \dot{\theta}}{nk}. \quad (27)$$

By comparing this result with Eq. (17), we see that, indeed, the phase velocity is equal to the synchronous velocity

$$v_s = V_{n,\ell}. \quad (28)$$

In what follows we will use the following notation for the initial phase and synchronous velocities

$$v_s(0) = V_{n,\ell}(0) = \frac{\ell \omega(t=0)}{n k} = \frac{\ell}{n} \frac{\lambda}{\tau(t=0)} = \frac{\ell}{n} V_0. \quad (29)$$

In order to derive an expression for the temporal phase consistent with the condition of a constant synchronous phase, we invoke Eq. (21)

$$\theta = \frac{nkz_s}{\ell} - \frac{\phi_s}{\ell} \quad (30)$$

and substitute for  $z_s$  from the first integral of Eq. (25)

$$z_s = \frac{1}{2} a_s t^2 + v_s(0)t + z_0 = \frac{1}{2} a_s t^2 + \frac{\ell}{n} V_0 t + \frac{\phi_s}{nk}, \quad (31)$$

where the initial position,  $z_0$ , was obtained from Eq. (24). This yields a temporal phase

$$\theta(t) = \frac{nkz_s}{\ell} - \frac{\phi_s}{\ell} = \frac{1}{2} \frac{n}{\ell} k a_s t^2 + k V_0 t - \frac{\phi_s}{nk}, \quad (32)$$

which pertains to a square wave that falls or rises only when the following periodic condition is fulfilled:

$$\theta(t) = \frac{1}{2} \frac{n}{\ell} k a_s t^2 + k V_0 t = q\pi \quad q = 0, 1, 2, \dots \quad (33)$$

Equation (33) defines exactly that switching sequence which is required in order to keep the phase of the synchronous molecule constant and hence for achieving a constant acceleration or deceleration. The corresponding switching times are given by solving Eq. (33) for  $t(q)$ , with the result

$$t(q) = \frac{\ell}{n} \frac{V_0}{a_s} \left[ \left( \frac{2\pi q n a_s}{k\ell V_0^2} + 1 \right)^{1/2} - 1 \right], \quad (34)$$

which is identical with a result obtained earlier [21]. We note that since we determine  $\theta(t)$ , via Eq. (33), before computing  $\omega(t)$  or  $\tau(t)$ , a need to evaluate the integration constant of Eq. (6) never arises.

Figure 2 shows a switching sequence, generated by Eq. (33), which is suitable for decelerating OH radicals.

#### D. Equation of motion

The equation of motion of a nonsynchronous molecule subjected to wave  $(n, \ell)$  is

$$\ddot{z} = \frac{F_{n,\ell}}{M} = A_{n,\ell} \sin \phi_{n,\ell}, \quad (35)$$

where we made use of Eq. (18). For the synchronous molecule we have

$$\ddot{z}_s = \frac{F_{n,\ell}}{M} = A_{n,\ell} \sin \phi_s. \quad (36)$$

A combination of Eqs. (35) and (36) yields

$$\ddot{z} - \ddot{z}_s = A_{n,\ell} (\sin \phi_{n,\ell} - \sin \phi_s). \quad (37)$$

The left-hand side of Eq. (37) can be recast in terms of the nonsynchronous and synchronous phase. We have, with the help of Eq. (19)

$$\begin{aligned} \phi_{n,\ell}(t) - \phi_s(t) &\equiv \Delta \phi_{n,\ell}(t) = nkz(t) - \ell \theta(t) - [nkz_s(t) - \ell \theta(t)] \\ &= nk[z(t) - z_s(t)] \equiv nk\Delta z(t), \end{aligned} \quad (38)$$

where  $\Delta z \equiv z - z_s$  is the longitudinal distance between the nonsynchronous and synchronous molecule, see also Fig. 3. Equation (38) implies the following equations for the time derivatives:

$$\dot{\phi}_{n,\ell}(t) - \dot{\phi}_s(t) \equiv \Delta \dot{\phi}_{n,\ell}(t) = nk(\dot{z} - \dot{z}_s) \equiv nk\Delta \dot{z} \quad (39)$$

and

$$\ddot{\phi}_{n,\ell}(t) - \ddot{\phi}_s(t) \equiv \Delta \ddot{\phi}_{n,\ell}(t) = nk(\ddot{z} - \ddot{z}_s) \equiv nk\Delta \ddot{z}. \quad (40)$$

However,

$$\Delta \dot{\phi}_{n,\ell}(t) = \dot{\phi}_{n,\ell}(t) \quad (41)$$

and

$$\Delta \ddot{\phi}_{n,\ell}(t) = \ddot{\phi}_{n,\ell}(t) \quad (42)$$

since, by definition,  $\dot{\phi}_s(t) = \ddot{\phi}_s(t) = 0$ .

Substituting Eqs. (40) and (42) into Eq. (37) finally yields

$$\ddot{\phi}_{n,\ell} = \alpha_{n,\ell} (\sin \phi_{n,\ell} - \sin \phi_s) \quad (43)$$

with

$$\alpha_{n,\ell} \equiv nkA_{n,\ell} = (-1)^{1/2(n+1)} \frac{2n^2 k^2}{\pi \ell M} W_n. \quad (44)$$

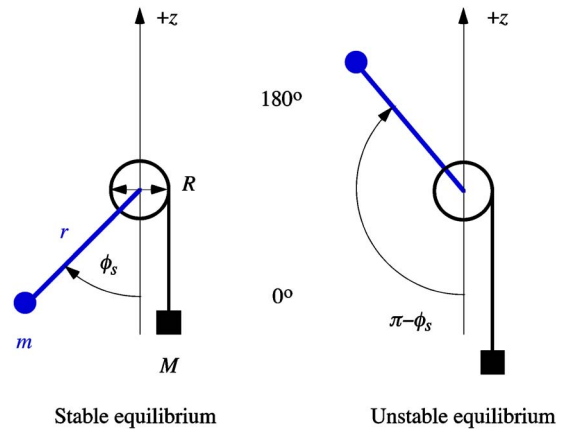


FIG. 4. (Color online) Realizations of a plane biased pendulum: a bob of mass  $m$  is fixed to a rigid suspension of length  $r$  which is attached to an axle of diameter  $R$ ; wound around the axle is a string that carries a bias of mass  $M$ . A plane biased pendulum is a one-dimensional system, whose only coordinate is the angle  $\phi$  between the vertical axis  $z$  and the bob suspension  $r$ . The stable and unstable equilibrium points are located symmetrically with respect to a plane perpendicular to the direction of the  $z$  axis at angles  $\phi_s$  and  $\pi - \phi_s$ , respectively. The stable-equilibrium angle  $\phi_s$  of the biased pendulum corresponds to the synchronous phase of the Stark accelerator/decelerator.

#### E. Solving the equation of motion

Relating the motion of all molecules to a molecule which maintains a constant (synchronous) phase with respect to a given wave not only greatly simplifies the equation of motion but reduces it to a form which is isomorphic with the equation of motion of a *biased pendulum*, see Fig. 4. Since the biased pendulum problem can be well understood—both mathematically and intuitively—it offers invaluable lessons about the Stark accelerator/decelerator dynamics [15].

Both the biased-pendulum problem and the Stark accelerator/decelerator have the following Lagrangian:

$$\mathcal{L}(\phi, \dot{\phi}) = \frac{1}{2} \eta \dot{\phi}^2 - \eta \alpha_{n,\ell} (\cos \phi + \phi \sin \phi_s), \quad (45)$$

where  $\eta$  and  $\alpha_{n,\ell}$  are constants different for the two problems. The application of Lagrange's equation

$$\frac{\partial \mathcal{L}}{\partial \phi} = \frac{d}{dt} \frac{\partial \mathcal{L}}{\partial \dot{\phi}} \quad (46)$$

immediately yields the correct equation of motion, namely Eq. (43).

The first term of the Lagrangian (45) is the kinetic energy, the second term is the potential

$$\begin{aligned} V(\phi) &= \eta \alpha_{n,\ell} (\cos \phi + \phi \sin \phi_s) \\ &= (-1)^{1/2(n+1)} \frac{2W_n}{\pi \ell} (\cos \phi + \phi \sin \phi_s) \\ &\equiv V_P(\phi) + V_B(\phi). \end{aligned} \quad (47)$$

In writing down the potential we split it into the pendulum part,  $V_P(\phi)$ , and the bias part,  $V_B(\phi)$ . These are plotted for

four different cases ( $\alpha_{n,\ell}$  positive/negative, acceleration/deceleration) in Fig. 5. The figure provides a valuable insight into the dynamics of the studied system(s). Like a simple pendulum, a biased pendulum has two equilibrium points, a *stable* and an *unstable* one, the latter called here a *tipping point*. These are located, symmetrically, at  $\phi = \phi_s$  and  $\phi = \pi - \phi_s$  and correspond to the positions of the minimum and maximum (modulo  $2\pi$ ) of the potential (47), as revealed by taking the first and second derivatives of the potential with respect to  $\phi$ , see also Ref. [15]. The unstable equilibrium point coincides with the outermost turning point,  $\phi_{out}$ . Angles in excess of  $\phi_{out}$  result in a nonuniform accelerating rotation of the pendulum about its axle, propelled by the falling bias. For the accelerator or decelerator this means that nonsynchronous molecules whose phase would exceed the tipping point will fall out of the potential well due to  $V(\phi)$  and thus be lost. Exceeding the tipping point amounts to disengaging from the acceleration or deceleration process. On the other hand, the inner turning point,  $\phi_{in}$ , cannot be exceeded, since the potential at  $\phi < \phi_{in}$  is repulsive. The phase of a nonsynchronous molecule that is confined by the potential periodically oscillates about the synchronous phase, whose value is set by the position of the potential's minimum. We also note that for higher acceleration or deceleration rates, the potential minimum shifts correspondingly and the well becomes shallower, see Fig. 6. This leads to a reduction and shifting of areas where stable oscillations of the nonsynchronous phase about the synchronous one can take place, i.e., the areas of the so-called *phase stability*. In what follows we will evaluate the phase-stable areas of the phase space exactly.

Multiplying the equation of motion (43)—where we dropped the  $n, \ell$  subscripts from the phase for notational simplicity—by  $\dot{\phi}$  and integrating once over time

$$\int \ddot{\phi} \dot{\phi} dt = \alpha_{n,\ell} \int \sin \phi \dot{\phi} dt - \alpha_{n,\ell} \int \sin \phi_s \dot{\phi} dt \quad (48)$$

yields

$$\dot{\phi}^2 = -2\alpha_{n,\ell}(\cos \phi + \phi \sin \phi_s) + \beta \quad (49)$$

or

$$\dot{\phi} = \pm [-2\alpha_{n,\ell}(\cos \phi + \phi \sin \phi_s) + \beta]^{1/2} \quad (50)$$

with  $\beta$  an integration constant. Equation (50) represents the trajectory of a nonsynchronous molecule through phase space  $(\dot{\phi}, \phi)$ .

For a bound motion,  $\beta$  is determined by the condition  $\dot{\phi}=0$ , which defines the value  $\phi_{out}$  of the nonsynchronous phase at the outer *turning point*, see Figs. 5 and 6. Thus

$$\beta = 2\alpha_{n,\ell}(\cos \phi_{out} + \phi_{out} \sin \phi_s). \quad (51)$$

A special case occurs when the turning point reaches its maximum, tipping value. This determines the *separatrix*, which separates the bound and unbound motion in the phase space. Along the separatrix,  $\dot{\phi}$  becomes zero at the nearest local maximum of the potential. We distinguish four cases,

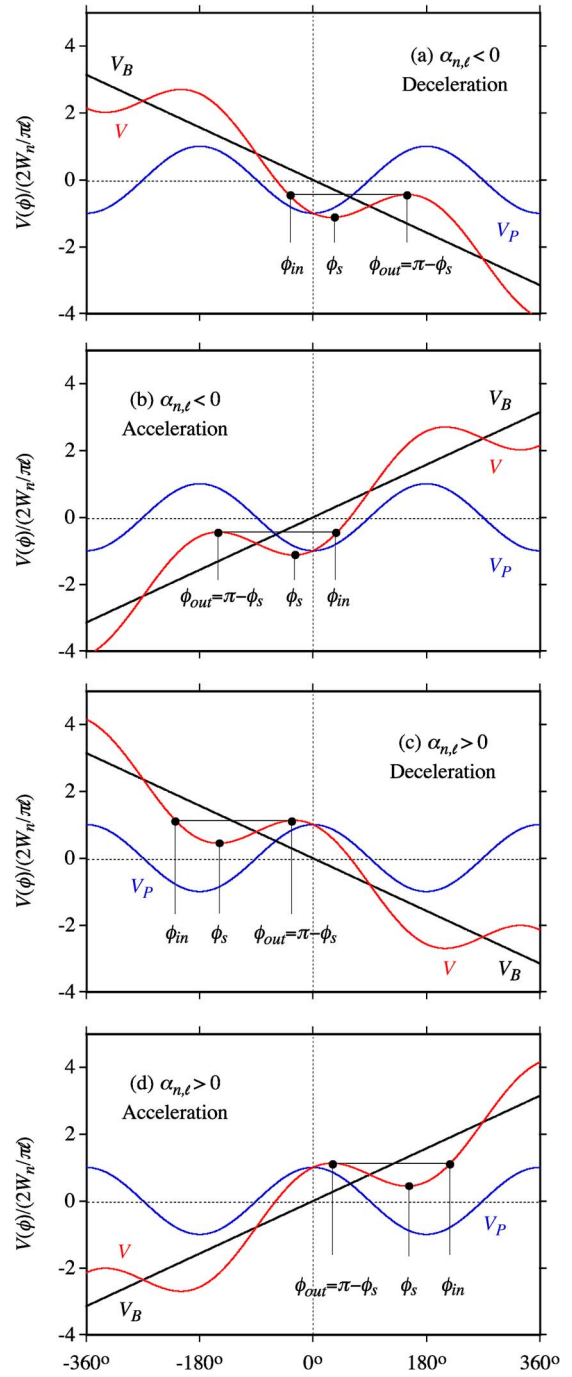


FIG. 5. (Color online) The potential  $V(\phi)$  of a biased pendulum or, interchangeably, of an accelerator/decelerator, Eq. (47) (red curve), along with the pure pendulum potential  $V_P(\phi)$  (blue curve) and the potential of the bias  $V_B(\phi)$  (black curve). Also shown are the minimum (stable) and maximum (unstable) equilibrium points. One can see that the unstable equilibrium point coincides with the outermost turning point,  $\phi_{out}$ , in the biased-pendulum potential. Angles in excess of  $\phi_{out}$  result in a nonuniform accelerating rotation of the pendulum about the axle, propelled by the falling bias. On the other hand, the inner turning point,  $\phi_{in}$ , cannot be exceeded, since the potential at  $\phi < \phi_{in}$  is repulsive. The cases of acceleration and deceleration for  $\alpha_{n,\ell} < 0$  and  $\alpha_{n,\ell} > 0$  are shown in panels (a)–(d), as labeled. The potential is expressed in terms of its amplitude  $\frac{2W_n}{\pi\ell}$ , see Eqs. (13) and (14).

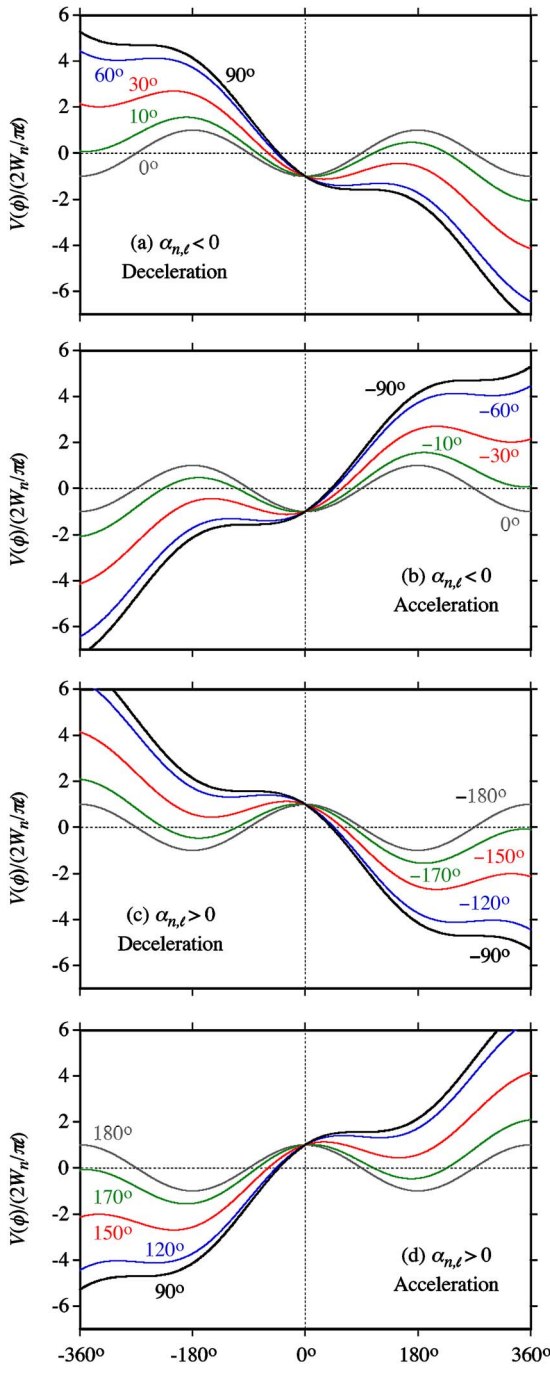


FIG. 6. (Color online) Biased pendulum or, interchangeably, Stark accelerator/decelerator potential  $V(\phi)$  for a range of values of the stable equilibrium point or, interchangeably, of the synchronous phase,  $\phi_s$ . For  $\phi_s = \pm \pi/2$ , the stable and unstable equilibrium points coincide and the potential cannot support any bound states. The potential is expressed in terms of its amplitude  $\frac{2W_n}{\pi\ell}$ , see Eqs. (13) and (14).

corresponding to the four different types of potentials shown in Figs. 5 and 6.

**Case 1:**  $\alpha_{n,\ell} < 0$ ,  $0 \leq \phi_s \leq \frac{\pi}{2}$  and  $-\pi \leq \phi \leq \pi$ , pertaining to deceleration.

Along the separatrix,  $\dot{\phi}$  becomes zero at  $\phi_{out} = \pi - \phi_s$ , see also Fig. 5(a). Using Eq. (51) we obtain for the corresponding  $\beta$

$$\beta = -2\alpha_{n,\ell}[\cos \phi_s - (\pi - \phi_s)\sin \phi_s]. \quad (52)$$

Inserting this into Eq. (50) gives the expression for the separatrix

$$\dot{\phi} = \pm [-2\alpha_{n,\ell}(\cos \phi + \cos \phi_s + (\phi - \pi + \phi_s)\sin \phi_s)]^{1/2}, \quad (53)$$

which is plotted for various values of  $\phi_s$  in Fig. 7(a). For the other cases we can follow exactly the same procedure.

**Case 2:**  $\alpha_{n,\ell} < 0$ ,  $-\frac{\pi}{2} \leq \phi_s \leq 0$  and  $-\pi \leq \phi \leq \pi$ , pertaining to acceleration.

Along the separatrix,  $\dot{\phi}$  becomes zero at  $\phi_{out} = -\pi - \phi_s$ ; see also Fig. 5(b). Here

$$\beta = -2\alpha_{n,\ell}[\cos \phi_s + (\pi + \phi_s)\sin \phi_s] \quad (54)$$

and the separatrix is given by

$$\dot{\phi} = \pm [-2\alpha_{n,\ell}(\cos \phi + \cos \phi_s + (\phi + \pi + \phi_s)\sin \phi_s)]^{1/2}, \quad (55)$$

which is plotted for various values of  $\phi_s$  in Fig. 7(b).

**Case 3:**  $\alpha_{n,\ell} > 0$ ,  $-\pi \leq \phi_s \leq -\frac{\pi}{2}$  and  $-2\pi \leq \phi \leq 0$ , pertaining to deceleration.

Along the separatrix,  $\dot{\phi}$  becomes zero at  $\phi_{out} = -\pi - \phi_s$ ; see also Fig. 5(c). Here

$$\beta = 2\alpha_{n,\ell}[-\cos \phi_s - (\pi + \phi_s)\sin \phi_s] \quad (56)$$

and so the separatrix is given by

$$\dot{\phi} = \pm [2\alpha_{n,\ell}(-\cos \phi - \cos \phi_s - (\phi + \pi + \phi_s)\sin \phi_s)]^{1/2} \quad (57)$$

which is plotted for various values of  $\phi_s$  in Fig. 7(c).

**Case 4:**  $\alpha_{n,\ell} > 0$ ,  $\frac{\pi}{2} \leq \phi_s \leq \pi$  and  $0 \leq \phi \leq 2\pi$ , pertaining to acceleration.

Along the separatrix,  $\dot{\phi}$  becomes zero at  $\phi_{out} = \pi - \phi_s$ ; see also Fig. 5(d). Here

$$\beta = 2\alpha_{n,\ell}[-\cos \phi_s + (\pi - \phi_s)\sin \phi_s] \quad (58)$$

and the separatrix is given by

$$\dot{\phi} = \pm [2\alpha_{n,\ell}(-\cos \phi - \cos \phi_s + (\pi - \phi - \phi_s)\sin \phi_s)]^{1/2}, \quad (59)$$

which is plotted for various values of  $\phi_s$  in Fig. 7(d).

For all other combinations of  $\alpha_{n,\ell}$  and  $\phi_s$  there is no phase stability, as also illustrated by Fig. 6. We note that  $\phi_s(\alpha_{n,\ell} < 0) \rightarrow \phi_s(\alpha_{n,\ell} > 0) - \pi$  for deceleration (cases 1 and 3) and  $\phi_s(\alpha_{n,\ell} < 0) \rightarrow \phi_s(\alpha_{n,\ell} > 0) + \pi$  for acceleration (cases 2 and 4).

## F. Small-angle dynamics

Equation (43) can be solved analytically for small phase oscillations, i.e., for  $\Delta\phi \ll 1$ . In that case

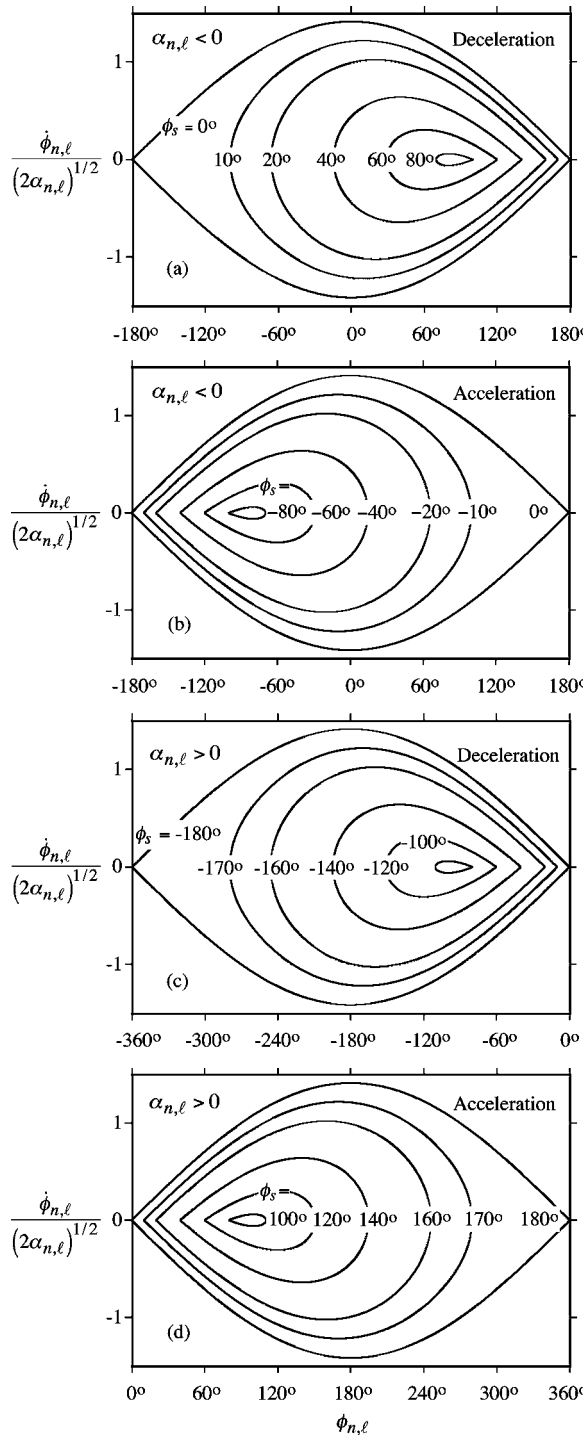


FIG. 7. The separatrices, determined from Eqs. (53), (55), (57), and (59), as functions of the synchronous phase,  $\phi_s$ . Contours demarcate domains in phase space  $(\dot{\phi}_{n,\ell}, \phi_{n,\ell})$  where stable oscillations take place. Note that  $\dot{\phi}_{n,\ell}/(2\alpha_{n,\ell})^{1/2}$  plays the role of a (dimensionless) momentum and the angle  $\phi$  of its conjugate coordinate. Depending on the sign of  $\alpha_{n,\ell}$  and on the sign of  $a_s$  (acceleration or deceleration), four cases are distinguished and shown in panels (a)–(d).

$$\begin{aligned} \sin \phi &= \sin(\Delta\phi + \phi_s) = \sin \phi_s \cos \Delta\phi + \cos \phi_s \sin \Delta\phi \\ &\approx \sin \phi_s + \Delta\phi \cos \phi_s \end{aligned} \quad (60)$$

and so Eq. (43) becomes

$$\Delta \ddot{\phi} \approx \alpha_{n,\ell} \Delta\phi \cos \phi_s, \quad (61)$$

which is recognized as the harmonic oscillator equation for  $\alpha_{n,\ell} < 0$  and  $-\pi/2 \leq \phi_s \leq \pi/2$  or for  $\alpha_{n,\ell} > 0$  and  $\pi/2 \leq \phi_s \leq 3\pi/2$ . Other combinations of  $\alpha_{n,\ell}$  and  $\phi_s$  lead to nonoscillatory, exponentially diverging solutions of Eq. (61), which preclude phase stability.

The harmonic solution of Eq. (61) is

$$\Delta\phi \approx \Delta\phi_0 \cos(\Omega t + \delta_0) \quad (62)$$

with

$$\Omega^2 \equiv -\alpha_{n,\ell} \cos \phi_s \equiv \Omega_{n,\ell}^2 \geq 0 \quad (63)$$

the angular frequency of the harmonic phase oscillations,  $\Delta\phi_0$  the initial phase difference, and  $\delta_0$  the initial temporal phase. The harmonic slow-oscillation frequency is given by

$$\frac{\Omega}{2\pi} = \left| \frac{2n^2 W_n}{\pi \ell M \lambda^2} \cos \phi_s \right|^{1/2}, \quad (64)$$

where we made use of Eqs. (44) and (63). This differs for  $n > 1$  from the result obtained previously [22].

Thus we see that for small relative phase angles,  $\Delta\phi$ , the nonsynchronous molecule oscillates harmonically about the synchronous one with a frequency  $\Omega$ . As  $\Delta\phi$  increases, the anharmonic terms in the sine expansion become more important and the small-angle approximation becomes invalid. The onset of the anharmonic terms brings about more complicated, lower-frequency oscillations. At the separatrix; the oscillation frequency drops to zero and beyond the separatrix the motion becomes unbound with no periodic phase oscillations.

At this juncture, we will make a general point which we will use frequently later on. We will refer to the oscillations of the nonsynchronous phase about the synchronous one as *slow oscillations*. This reflects the fact that  $\Omega$  is typically much smaller than  $\omega(t)$ . In contradistinction, we will refer to the oscillations at frequency  $\omega(t)$  as *fast oscillations*.

We note that the period  $T_{n,\ell}$  of the (slow) oscillations is generally given by

$$T_{n,\ell} = 2 \int_{\phi_{in}}^{\phi_{out}} \frac{dt}{d\phi_{n,\ell}} d\phi_{n,\ell} \quad (65a)$$

and can be evaluated numerically from the first integral of the equation of motion (43) and from the transcendental equations for the turning points  $\phi_{in} \equiv \phi_{in}^{n,\ell}$  and  $\phi_{out} \equiv \phi_{out}^{n,\ell}$ . For harmonic oscillations

$$T_{n,\ell} = \frac{2\pi}{\Omega_{n,\ell}} \quad (66a)$$

## G. Phase stability

The notion of *phase stability* pertains to periodic solutions of the equation of motion (43). Physically, these correspond

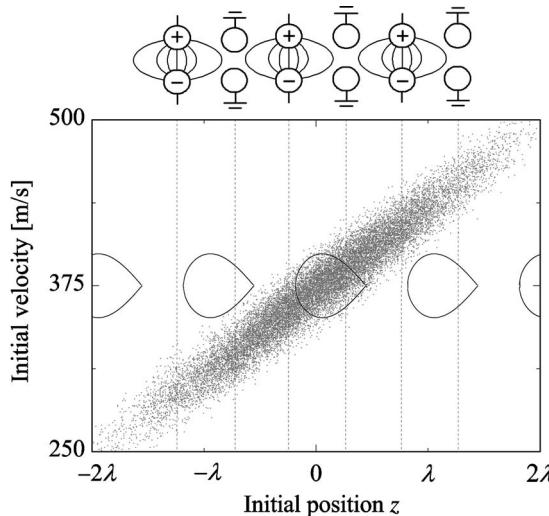


FIG. 8. Phase-space distribution of a molecular beam as it enters a Stark accelerator/decelerator. The best overlap between a phase stable area (black fishes) and the molecular beam pulse (swarm of dots) is obtained when the synchronous molecule matches the mean position and velocity of the beam molecules. Cf. Fig. 2.

to stable oscillations of the nonsynchronous molecule about the synchronous one. The solutions of the equation of motion, given by Eqs. (53), (55), (57), and (59), determine a boundary for the momentum of the nonsynchronous molecule,  $\dot{\phi}_{n,\ell}$ , as a function of its phase,  $\phi_{n,\ell}$ , that pertains to phase-stable motion. That is to say, together,  $(\dot{\phi}_{n,\ell}, \phi_{n,\ell})$  delimit an *area of phase stability in the phase space* for molecules interacting with a given wave  $(n, \ell)$ .

Phase stability is a key property of a Stark accelerator or decelerator, which enables handling other molecules than just the synchronous one. This is what makes the device a practical one, since *bunches* of molecules, with a *distribution of positions and velocities*, can then be accelerated or decelerated. Without phase stability, only a single molecule could be handled, namely the synchronous one [23,24].

The explicit evaluation of the phase-stable areas, Eqs. (53), (55), (57), and (59), clarifies several issues:

(a) The *choice of the synchronous molecule*. The distribution of positions and velocities of molecules in a bunch (typically Gaussian, for a pulsed supersonic beam, Ref. [25]) occupies a certain region of phase space. In order for the accelerator or decelerator to act on most of the molecules in the bunch, an overlap between the phase space occupied by the bunch and the separatrices for phase-stable acceleration or deceleration needs to be sought. As the calculations of the separatrices attest, the synchronous molecule is always at the center of the phase-stable area, cf. Fig. 7. Hence a maximum phase-space overlap is achieved when the position and velocity of the synchronous molecule coincides with the most probable position and velocity of the molecular-beam pulse, see Fig. 8. Thus in an acceleration or deceleration experiment, the synchronous molecule is generally defined by the most probable position and velocity of the molecular-beam pulse.

(b) The *size of the phase-stable areas* depends on  $\phi_s$  which, in turn, determines the *acceleration or deceleration*

*rate*. At higher deceleration rates, only smaller bunches of molecules can be handled. The largest bunches of molecules can be handled at zero deceleration, when a bunch is just transported (i.e., guided) through the field array.

(c) The *dominant wave*. Since  $\varepsilon_1$  is the largest spatial Fourier coefficient, cf. Eq. (11), we see that  $\alpha_{11}$  supports the largest phase-stable area and affords the highest acceleration or deceleration rate. The corresponding wave,  $(+, 1, 1)$ , referred to as the *first-harmonic wave*, gives the best yield according to this 1D treatment. *Higher overtones* are normally not used in experiments, but the effects of many have been observed [16]. In Sec. V we will examine in more detail the relative sizes of the phase-stable areas due to different overtones.

## H. Why does a single wave do nearly the whole job ?

So far we limited our considerations to the single-wave dynamics, i.e., to the equation of motion and its solutions that pertain to a single wave  $(\pm, n, \ell)$  interacting with a bunch of molecules. Here we will show that it is indeed just a single wave that gives a ride to molecules, with the infinitely many other waves, Eq. (15), playing no role or a marginal one (see Sec. V C on interferences).

In order to see why this is the case, we will look at the effect an arbitrary perturbing wave  $(+, r, s)$  has on the phase-stable motion of molecules due to a  $(+, n, \ell)$  wave, whose dynamics we outlined in Sec. IV.

Before delving into that, however, let us consider first the relationship between the velocities of the nonsynchronous and synchronous molecules for an arbitrary single wave. Since the averages of the nonsynchronous phase and its time derivatives over the oscillation period  $T_{n,\ell}$  are identically equal to zero

$$\langle \dot{\phi}_{n,\ell} \rangle \equiv \frac{1}{T_{n,\ell}} \int \dot{\phi}_{n,\ell} dt = 0 \quad (67)$$

and since, from Eq. (39),

$$\Delta \dot{z} = \dot{z} - \dot{z}_s = v - v_s = nk \Delta \dot{\phi}_{n,\ell} = nk \dot{\phi}_{n,\ell}, \quad (68)$$

we see that

$$\begin{aligned} \langle v - v_s \rangle &= \frac{1}{T_{n,\ell}} \int (v - v_s) dt = \frac{1}{T_{n,\ell}} \int v dt - \frac{1}{T_{n,\ell}} \int v_s dt \\ &= \langle v \rangle - \langle v_s \rangle = nk \langle \dot{\phi}_{n,\ell} \rangle = 0, \end{aligned} \quad (69)$$

i.e., the nonsynchronous velocity averaged over a phase oscillation is equal to the average synchronous velocity. This in turn shows that the synchronous velocity (pertaining to a given wave) acts as a *pilot* for the nonsynchronous velocity (pertaining to that same wave) as long as phase stability is maintained. Therefore, *molecules which periodically oscillate about a molecule synchronous with an arbitrary wave will get a ride from that wave!* In what follows we will call a wave that gives a ride to a given bunch of molecules a *resonant wave*.

Let us now approach the problem from the other side and look at the effect of a perturbing wave on the motion driven

by a resonant wave. We will look at the case of zero acceleration, i.e., the case when the switching frequency  $\omega$  is constant and the Stark accelerator/decelerator serves as a *guide*. This will make our calculations simpler, although the same arguments would apply to the general case of nonzero acceleration. Also, we will make our notation more accurate and, invoking Eqs. (17) and (19), write the molecule's coordinate as

$$z_{n,\ell} = \frac{\phi_{n,\ell}}{nk} + \frac{\ell}{n} V_0 t. \quad (70)$$

The acceleration of a molecule whose motion is resonant with the  $(+, n, \ell)$  wave is given by

$$\ddot{z}_{n,\ell} = \frac{F_{n,\ell}}{M} = A_{n,\ell} \sin \phi_{n,\ell} = A_{n,\ell} \sin(nkz_{n,\ell} - \ell\omega t), \quad (71)$$

where we made use of Eqs. (19), (35), and (70). For small oscillations, the unperturbed coordinate of a molecule riding the  $(+, n, \ell)$  wave is

$$z_{n,\ell}(t) = \frac{\Delta\phi_0}{nk} \cos(\Omega_{n,\ell}t + \delta_0) + \frac{\ell}{n} V_0 t + \frac{\phi_s}{nk} \quad (72)$$

as follows from Eqs. (38), (62), and (70); its velocity, obtained by taking the time derivative of Eq. (72), is

$$v_{n,\ell}(t) = \frac{\ell}{n} V_0 - \frac{\Delta\phi_0 \Omega_{n,\ell}}{nk} \sin(\Omega_{n,\ell}t + \delta_0). \quad (73)$$

The harmonic slow-oscillation frequency  $\Omega_{n,\ell}$  is given by Eq. (63).

We will consider now the perturbing effect of the  $(+, r, s)$  wave on the motion of a molecule which is riding the  $(+, n, \ell)$  wave. The  $(+, r, s)$  wave perturbs the ride of the molecule by acting on its coordinate  $z_{n,\ell}$  as determined by the  $(+, n, \ell)$  wave. Thus the acceleration imparted to a molecule by the perturbing  $(+, r, s)$  wave is

$$\begin{aligned} \ddot{z}_{n,\ell} &= \frac{F_{n,\ell}^{r,s}(t)}{M} \\ &= A_{r,s} \sin(rkz_{n,\ell}(t) - s\omega t) = A_{r,s} \sin\left[\frac{r}{n} \phi_{n,\ell} - \omega_{n,\ell}^{r,s} t\right], \end{aligned} \quad (74)$$

where we made use of Eq. (70) and introduced the frequency

$$\omega_{n,\ell}^{r,s} \equiv \frac{ns - \ell r}{n} \omega \equiv \frac{2\pi}{\tau_{n,\ell}^{r,s}}, \quad (75)$$

which is a fast-oscillation frequency, since it is on the order of  $\omega$ . Clearly, the time average of the perturbing force  $F_{n,\ell}^{r,s}$  over the perturbation period  $\tau_{n,\ell}^{r,s}$  vanishes

$$\langle F_{n,\ell}^{r,s} \rangle \equiv \frac{1}{\tau_{n,\ell}^{r,s}} \int F_{n,\ell}^{r,s} dt = 0 \quad (76)$$

as follows by substitution of Eq. (74) into Eq. (76) and integration, under the assumption that the slowly oscillating phase  $\phi_{n,\ell}$  remains constant over the period  $\tau_{n,\ell}^{r,s}$ . Hence the perturbing force is seen to average out fast, as a result of

which the perturbing wave has no *net* effect on the phase-stable motion of the molecule.

The velocity,  $v_{n,\ell}^{r,s}$ , and the displacement,  $z_{n,\ell}^{r,s}$ , imparted by the perturbing wave can be obtained by integrating Eq. (74). Integrating once (under the assumption of  $\phi_{n,\ell}$  constant) yields the instantaneous velocity due to the perturbing wave

$$v_{n,\ell}^{r,s}(t) = \frac{1}{\omega_{m,\ell}^{r,s}} A_{r,s} \cos\left[\frac{r}{n} \phi_{n,\ell} - \omega_{n,\ell}^{r,s} t\right]. \quad (77)$$

Integrating once more gives the displacement caused by the perturbing force

$$z_{n,\ell}^{r,s} = -\frac{1}{(\omega_{n,\ell}^{r,s})^2} A_{r,s} \sin\left[\frac{r}{n} \phi_{n,\ell} - \omega_{n,\ell}^{r,s} t\right]. \quad (78)$$

Thus the effect of the perturbing wave on the velocity and on the displacement of the resonant wave is suppressed by  $\omega_{n,\ell}^{r,s}$  and  $(\omega_{n,\ell}^{r,s})^2$ , respectively. We see that the net effect of the perturbing wave vanishes because the perturbing wave fails to displace the molecule. This is indeed the reason why, to an excellent approximation, we are allowed to single out the resonant wave and handle it separately from the perturbing one(s). It is also the reason why a perturbing wave has no influence on phase stability.

The motion of a molecule resonant with the  $(+, n, \ell)$  wave and perturbed by the  $(+, r, s)$  wave can now be easily evaluated (for the case of small oscillations) by simply adding Eqs. (72) and (78) or (73) and (77), respectively. This analytic result can be compared with the result of a numerical integration of the differential equation for a nonsynchronous molecule interacting with the  $(+, n, \ell)$  and  $(+, r, s)$  waves. For example, for the  $(+, 1, 1)$  and  $(+, 3, 5)$  waves, the equation is

$$\ddot{z} = A_{11} \sin(kz - \omega t) + A_{35} \sin(3kz - 5\omega t) \quad (79)$$

and Fig. 9 shows the result of the corresponding numerical integration. The initial conditions are chosen such that the molecule interacts resonantly with the  $(+, 3, 5)$  wave, which means that the  $(+, 1, 1)$  wave acts as a nonresonant, perturbing wave. Since the  $(+, 1, 1)$  wave dominates the right-moving waves and since its phase velocity is close to  $(+, 3, 5)$  wave, the perturbing effect of the  $(+, 1, 1)$  wave is much larger than the effect of all the other waves in the Fourier expansion, Eq. (15). And yet, this perturbing effect is seen to be strongly suppressed because of the fast oscillations with respect to the  $(+, 3, 5)$  wave. While the perturbation of the velocity is still noticeable on a short time scale, see Fig. 9(a), the perturbation of the coordinate amounts to just a ripple, see Fig. 9(b). We note that the frequency and amplitude of the fast oscillations are correctly predicted by Eqs. (77) and (78), which reconfirms the validity of the assumptions used in the analysis of the perturbations.

In the case of acceleration or deceleration, the switching frequency is not constant, but increases or decreases linearly with time throughout the acceleration or deceleration process. Nevertheless, the treatment of the perturbations for the case of guiding, as given above in this paragraph, remains in

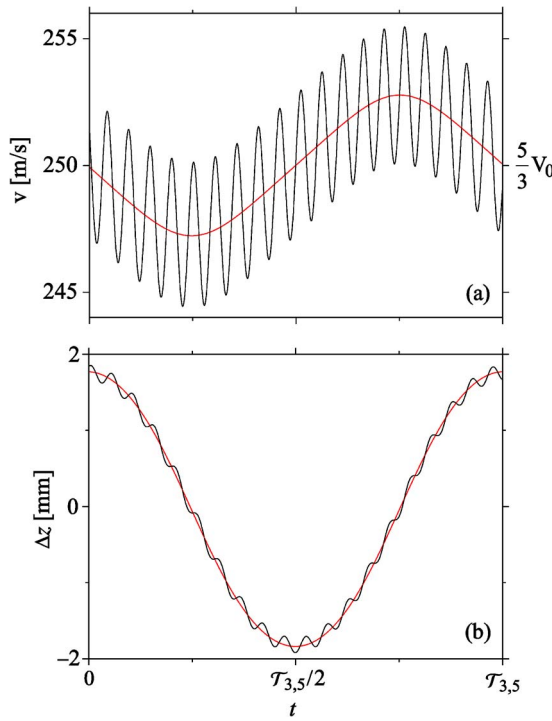


FIG. 9. (Color online) Dynamics of a nonsynchronous molecule riding the (3, 5) wave and perturbed by the (1, 1) wave. The dynamics was determined by numerically integrating the differential equation of the molecule interacting with the two waves, for initial conditions that make the (3, 5) wave resonant and the (1, 1) wave perturbing. Both the longitudinal velocity,  $v(t)$ , panel (a), and the longitudinal position,  $z(t) - v_s t$ , relative to the synchronous molecule moving at a velocity  $v_s$ , panel (b), exhibit slow oscillations superposed by fast oscillations. The slow oscillations arise from the single-wave interaction of the molecule with the resonant (3, 5) wave and are described by Eqs. (72) and (73). The fast oscillations are due to the perturbing (1, 1) wave and are described by Eqs. (77) and (78). While the influence of the nonresonant wave on the velocity is significant, its effect on the position  $z(t)$  is strongly suppressed. The time scale is given in terms of the slow-oscillation period  $\mathcal{T}_{n,\ell}$ .

place for this case as well, since  $\omega(t)$  essentially does not change during a fast-oscillation period (typically by less than 1%) and so can be treated as a constant.

The above treatment only breaks down in the limit  $\omega(t)=kV(t)\rightarrow 0$ , where the used assumption  $\omega(t)\ll\Omega$  no longer holds. In practice, such a situation does not occur, since even if the molecules are decelerated to velocities conducive to trapping, see Ref. [9],  $\omega(t)$  still considerably exceeds  $\Omega$ , and so the treatment remains in place.

### I. Two (or more) waves traveling with the same phase velocity

When the resonant and perturbing waves travel at the same phase velocity (i.e., for  $\ell/n=s/r=\kappa\ell/\kappa n$ , with  $\kappa$  an odd integer), the perturbing force, Eq. (74), does *not* average out. In this case one cannot speak of resonant and nonresonant waves, because all the waves which travel at this same velocity are equally resonant and will jointly create phase

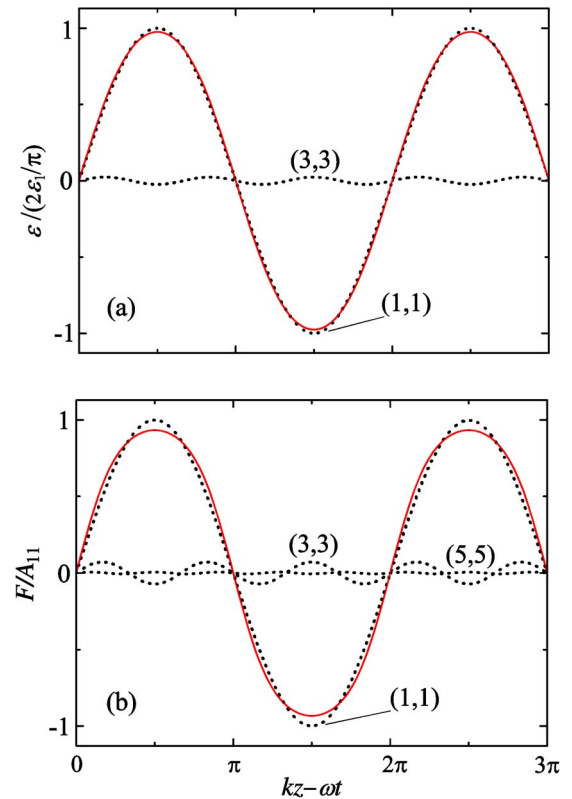


FIG. 10. (Color online) (a) Relative magnitude of the electric fields due to the (1, 1) wave and the (3, 3) wave (black dotted curves), which are traveling at the same velocity. These relative magnitudes are typical for two waves with successive  $n$  and the same velocity. We see that the net field (red curve) is determined predominantly by the (1, 1) wave, i.e., the one with the smaller value of  $n$ . The conclusions about phase stability can be reached by considering solely this wave. (b) Typical relative magnitudes of the force due to the (1, 1), (3, 3), and (5, 5) waves (black dotted curves), which are all traveling at the same velocity. Since a small deviation in the force can accumulate when calculating a switching sequence comprising many stages, one should rely on the net force (red curve) rather than on the dominant term, cf. Eq. (80).

stability. Since, obviously, any  $(+,n,\ell)$  wave has such fellow-traveler waves  $(+,\kappa n,\kappa \ell)$ , this is actually the usual situation. Figure 10(a) shows typical relative sizes of two waves with successive  $n$ , traveling at the same velocity. We see that the resulting shape of the well is dominated by one of the two waves, namely the one with the smaller  $n$ , cf. Eq. (11). Hence in order to draw conclusions about phase stability (which is determined by the shape and depth of the well), we can rely solely on the properties of the *dominant wave*.

However, when calculating switching sequences accurately, the influence of the nondominant wave(s) cannot be fully dismissed, because of the effect it has on the acceleration  $a_s$  (typically, a deviation of a few percent with respect to a single-wave treatment can accumulate over 100 acceleration/deceleration stages). Thus when evaluating the acceleration on a dominant  $(+,n,\ell)$  wave, one should replace Eq. (23) with the sum

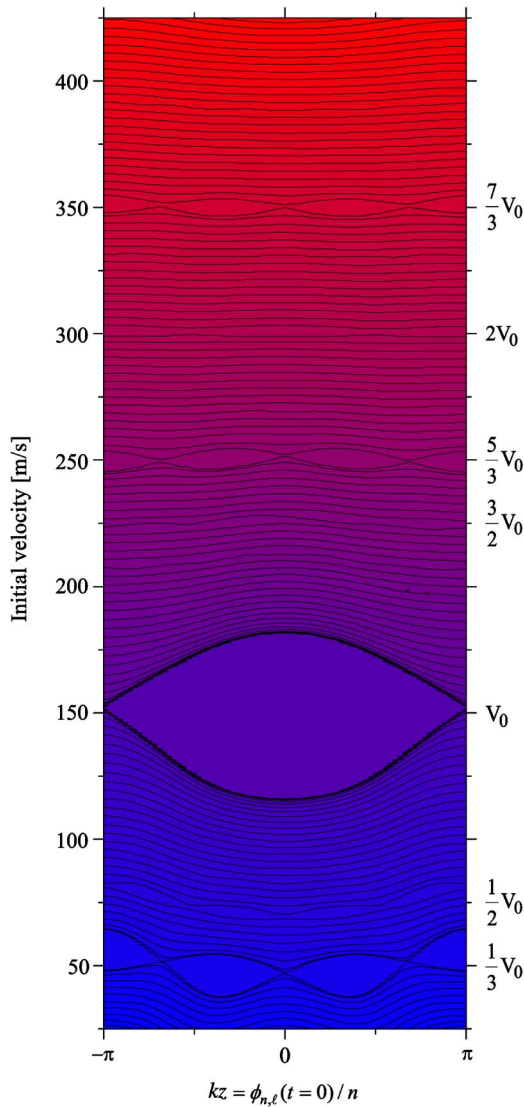


FIG. 11. (Color online) Global phase portrait showing the phase stable areas due to the various waves (case of guiding). The contours pertain to average velocities of OH molecules plotted as a function of their initial velocity  $v$  and initial spatial phase  $kz$ ; the link between the average velocity and phase stability is given by Eq. (69). The contour plot is obtained by numerically integrating the full equation of motion (81) for 80 waves with a temporal phase and switching sequence given, respectively, by Eqs. (32) and (33) corresponding to guiding ( $\sin \phi_s = 0$ ) at  $V_0 = 150$  m/s. The phase portrait is in perfect agreement with Monte Carlo trajectory simulations which, in turn, are in perfect agreement with experiment.

$$a_s = \sum_{\kappa \text{ odd}}^{\infty} A_{kn,\kappa\ell} \sin(\kappa\phi_s). \quad (80)$$

Note that this sum converges very fast, cf. Eqs. (14) and (16). Figure 10(b) shows, for the case of the (+,1,1) dominant wave, the modification of the force due to the presence of the resonant nondominant waves. We note that in order to achieve an accurate correspondence between  $a_s$  and  $\phi_s$ , several terms in Eq. (80) may have to be taken into account.

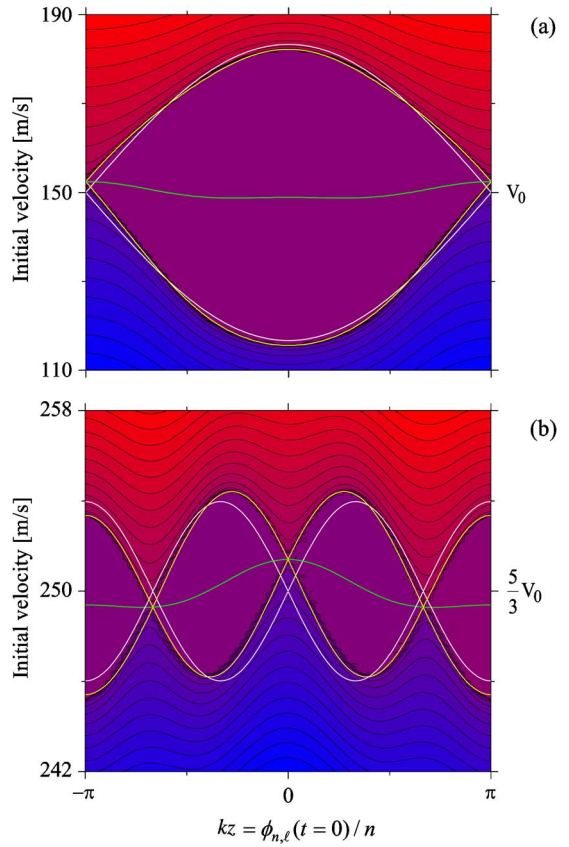


FIG. 12. (Color online) Detailed view of the phase stable areas of Fig. 11 around (a)  $V_0$  and (b)  $\frac{5}{3}V_0$  (the case of guiding). The contours pertain to average velocities of OH molecules plotted as a function of their initial velocity  $v$  and initial spatial phase  $kz$ . Zooming in at the global phase portrait allows for an accurate comparison of the full-fledged numerical result with the analytic treatment of the dynamics. The white curves show the separatrices calculated from Eqs. (86) and (87) for a resonant, single-wave interaction. The green curves are obtained from Eq. (89) and comprise the perturbations due to all the other, nonresonant waves. The yellow curves combine the two and are seen to render a perfect agreement with the full-fledged calculation.

## V. FULL-FLEDGED DYNAMICS

In Sec. IV H, we discussed the dynamics due to a single resonant wave perturbed by a single nonresonant wave. However, the exact (longitudinal) force that is acting on the molecules, Eq. (15), is due to infinitely many partial waves, out of which all but one are nonresonant (notwithstanding the discussion of Sec. IV I). In order to fully assess the role of the resonant wave *vis à vis* the nonresonant waves, we evaluated the combined effect due to a large number of waves and compared it with a single-wave effect. The single-wave dynamics, the full-fledged dynamics and the correction that needs to be applied to the single-wave dynamics in order to reproduce the full-fledged dynamics can be best visualized in a phase-space diagram. Such a diagram, or *phase portrait*, exemplified in Fig. 11, shows the average velocities of the molecules as a function of their initial velocity and initial spatial phase. The link between the average velocity and phase stability is given by Eq. (69). Note that in the phase

space regions corresponding to phase stability all the molecules have the same average velocity. The velocities that the contours correspond to can be read off from the velocity scale on the right.

The cases of guiding and of acceleration or deceleration due to a single wave will be described separately in Secs. V A and V B. Single-wave dynamics gives rise to features which occur at odd-fraction multiples,  $\ell/n$ , of the fundamental velocity  $V_0$ . In Sec. V C we will deal with features which occur at even-fraction multiples of the fundamental velocity  $V_0$ . These features arise from the interference of (typically) two adjacent waves.

### A. Guiding

The phase portrait shown in Fig. 11 was obtained from a numerical integration of the full equation of motion

$$\ddot{z}(t) = \frac{F(z,t)}{M} \quad (81)$$

with  $F(z,t)$  given by Eq. (15) and the temporal phase of the waves given by Eq. (32) with  $\sin \phi_s = 0$  corresponding to guiding. We found that increasing the number of waves included in the computation beyond 80 ( $n \leq 5, \ell \leq 25$ ) did not lead to any changes of the phase portraits in the range of the initial velocities and positions shown. Moreover, we found that the phase portrait of Fig. 11 agrees perfectly well with the one obtained from trajectory simulations which, in turn, perfectly reproduces experiment [16]. Therefore, for all intents and purposes, the phase portrait of Fig. 11 can be considered to be *exact*. The phase portrait captures all the complexity of the dynamics in question and makes it possible to see at a glance the phase-stable areas due to various waves. We remind ourselves of the fact that while the spatial Fourier components of  $F(z,t)$  decrease exponentially with increasing  $n$ , the temporal Fourier components decrease only as  $\ell^{-1}$ . Therefore, phase-stable areas corresponding to waves with  $n > 3$  can hardly be discerned but those with  $\ell \leq 7$  can still be easily observed in the phase-space area depicted.

Figure 12 shows in panels (a) and (b) detailed views of the phase-stable areas due to the first harmonic wave (+, 1, 1) and due to the (+, 3, 5) wave (note that  $\alpha_{11} < 0$  and  $\alpha_{35} > 0$  for the example of low-field seeking states considered here). The main features can be understood, for the case of guiding, from Eqs. (53) and (57), respectively. Before we apply these, we realize that, generally, the phase  $\phi_{n,\ell}$ , Eq. (19), yields a molecular velocity

$$v_{n,\ell} = \frac{\dot{\phi}_{n,\ell}}{nk} + \frac{\ell}{n} V_0 \quad (82)$$

and an initial position of the molecule

$$z_{n,\ell} = \frac{\phi_{n,\ell}}{nk} \quad \text{at } t = 0. \quad (83)$$

Equation (53) and (57), simplified for the case of guiding, become

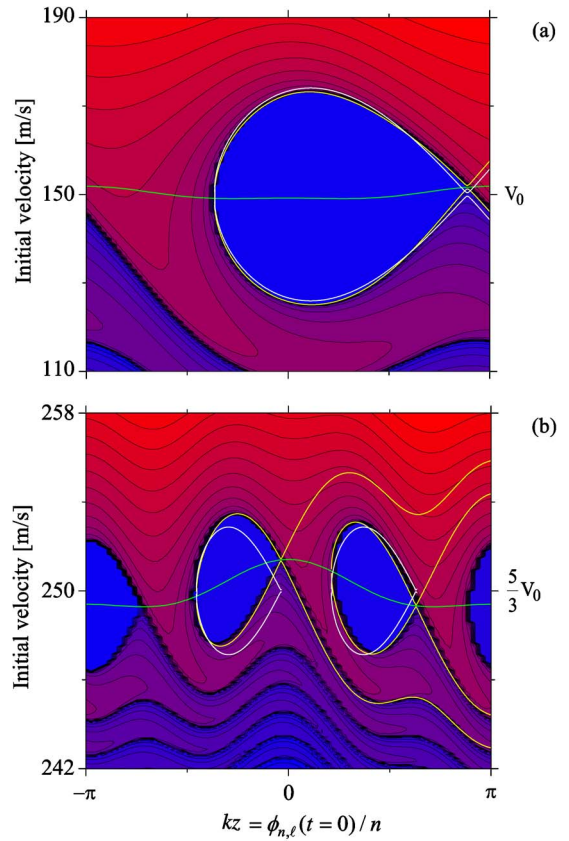


FIG. 13. (Color online) Detailed view of the phase stable areas around (a)  $V_0$  and (b)  $\frac{5}{3}V_0$  for the case of deceleration. The contours pertain to average velocities of OH molecules plotted as a function of their initial velocity  $v$  and initial spatial phase  $kz$ . The contours were obtained by numerically integrating the equation of motion (81) for 80 waves, with a temporal phase and switching sequence given, respectively, by Eqs. (32) and (33) corresponding to deceleration ( $A_{n,\ell} \sin \phi_s < 0$ ). Panel (a) shows the full-fledged numerical calculation for deceleration on the first-harmonic (1, 1) wave with  $\phi_s = 20^\circ$ . Panel (b) shows the full-fledged numerical calculation for deceleration on the (+, 3, 5) wave with  $\phi_s = -170^\circ$ . The white curves pertain to the separatrices obtained for a resonant, single-wave interaction, as given by Eqs. (53) and (57). The green curves are obtained from Eq. (89) and comprise the perturbations due to all the other, nonresonant waves. The yellow curves combine the two and are seen to be in perfect agreement with the full-fledged calculation.

$$\dot{\phi}_{n,\ell} = \pm [-2\alpha_{n\ell}(\cos \phi_{n,\ell} + 1)]^{1/2} \quad \alpha_{n\ell} < 0 \quad (84)$$

and

$$\dot{\phi}_{n,\ell} = \pm [2\alpha_{n\ell}(-\cos \phi_{n,\ell} + 1)]^{1/2} \quad \alpha_{n\ell} > 0. \quad (85)$$

Their combinations with Eq. (82) give the separatrices

$$v_{n,\ell} = \pm \frac{[-2\alpha_{n\ell}(1 + \cos \phi_{n,\ell})]^{1/2}}{nk} + \frac{\ell}{n} V_0 \quad (86)$$

and

$$v_{n,\ell} = \pm \frac{[2\alpha_{n\ell}(1 - \cos \phi_{n,\ell})]^{1/2}}{nk} + \frac{\ell}{n} V_0 \quad (87)$$

for the cases represented by waves (+, 1, 1) and (+, 3, 5), respectively. The separatrices obtained from Eqs. (86) and (87) are shown in Fig. 12 by the white curves. The equations capture all the qualitative features of the respective phase-stable areas seen in Figs. 11 and 12: (1) the phase-stable areas occur at velocities  $\frac{\ell}{n}V_0$ ; (2) the velocity (i.e., vertical) width of a phase-stable area for a given  $n$  is proportional to  $\ell^{-1/2}$ , because  $|\alpha_{n\ell}| \propto \ell^{-1}$ , Eq. (44); (3) the velocity width of a phase-stable area for a given  $\ell$  is proportional to  $\exp(-\frac{1}{2}\xi n)$ , cf. Eqs. (11) and (44); (4) when the spatial phase,  $kz_{n,\ell}$ , varies between  $-\pi$  and  $\pi$ , then the initial phase  $\phi_{n,\ell}(t=0) = nkz_{n,\ell}$  varies between  $-n\pi$  and  $n\pi$ ; as a result, the phase-stable area corresponding to an  $(\pm, n, \ell)$  wave consists of  $n$  “fishes” when the (horizontal) initial  $kz_{n,\ell} = \phi_{n,\ell}(t=0)/n$  spans the interval of  $-\pi$  to  $\pi$ ; (5) for  $\alpha_{n\ell} < 0$ , the nodes occur at  $kz_{n,\ell} = \pm\pi, \pm\pi \mp \frac{2\pi}{n}, \pm\pi \mp \frac{4\pi}{n}, \dots$ ; for  $\alpha_{n\ell} > 0$ , the nodes occur at  $kz_{n,\ell} = 0, \pm\frac{2\pi}{n}, \pm\frac{4\pi}{n}, \dots$

A closer inspection of Fig. 12 reveals that the agreement between the separatrix obtained from either Eq. (86) or Eq. (87) with the exact phase portrait is not perfect. The agreement can be improved to the point of perfection by correcting for the effect of the nonresonant waves. This we do by applying the approach developed for a single perturbing wave in Sec. IV H to all the perturbing waves, starting with Eq. (15). As a result

$$\begin{aligned} \tilde{v}_{n,\ell}(z, t) \equiv & \sum_{r \text{ odd}} \sum_{s \text{ odd}} v_{n,\ell}^{r,s}(t) = \sum_{r \text{ odd}} \sum_{s \text{ odd}} \frac{n}{\omega(ns - \ell r)} A_{r,s} \\ & \times \cos \left[ \frac{r}{n} \phi_{n,\ell} - \frac{\omega(ns - \ell r)}{n} t \right] \\ & + \sum_{r \text{ odd}} \sum_{s \text{ odd}} \frac{n}{\omega(ns + \ell r)} A_{r,s} \\ & \times \cos \left[ \frac{r}{n} \phi_{n,\ell} + \frac{\omega(ns + \ell r)}{n} t \right] - \sum_{p \text{ even}} \frac{n}{p \ell \omega} A_p \\ & \times \cos \left[ \frac{p}{n} (\phi_{n,\ell} + \ell \omega t) \right], \end{aligned} \quad (88)$$

where  $\tilde{v}_{n,\ell}$  is the velocity change of the molecules riding the resonant  $(+, n, \ell)$  wave due to the effect of all the nonresonant waves (so the summation is over all  $r, s = 1, 3, \dots$  for which  $ns - \ell r \neq 0$ ). Truncating the summation at  $r=1$  and  $p=2$ , we obtain for  $t=0$

$$\begin{aligned} \tilde{v}_{n,\ell}(z, t=0) \approx & \sum_{s \text{ odd}} \frac{n}{(ns - \ell) \omega} A_{1s} \cos(kz) \\ & + \sum_{s \text{ odd}} \frac{n}{(ns + \ell) \omega} A_{1s} \cos(kz) - \frac{n}{2\ell \omega} A_2 \cos(2kz). \end{aligned} \quad (89)$$

This is shown by the green line in Fig. 12 for  $s \leq 21$ . The yellow line shows the velocity  $v_{n,\ell}(z, t=0) + \tilde{v}_{n,\ell}(z, t=0)$ , and is seen to be in full agreement with the phase-stable area

obtained from the full-fledged calculation. No correction was needed for the position  $z_{n,\ell}$ , as the effect of the nonresonant waves is diminished by a factor proportional to  $\omega^2$ , see Eq. (78) and Fig. 9(b), and so does not show on the scale of the figure.

## B. Acceleration or deceleration

The phase portraits obtained for guiding can be easily generalized to the case of acceleration or deceleration, by incorporating in the numerical calculations a temporal phase, Eq. (32), corresponding to an accelerating or decelerating wave. Figure 13 attests to this being the case: panels (a) and (b) show the same parts of the phase space as panels (a) and (b) in Fig. 12, but for  $\phi_s = 20^\circ$  and  $\phi_s = -170^\circ$ , respectively, and both for deceleration. The white curves show the separatrices

$$v_{n,\ell}(t)$$

$$\begin{aligned} & = \pm \frac{[-2\alpha_{n\ell}(\cos \phi_{n,\ell} + \cos \phi_s + (\phi_{n,\ell} - \pi + \phi_s)\sin \phi_{n,\ell})]^{1/2}}{nk} \\ & + \frac{\ell}{n} V(t) \end{aligned} \quad (90)$$

and

$$v_{n,\ell}(t)$$

$$\begin{aligned} & = \pm \frac{[2\alpha_{n\ell}(-\cos \phi_{n,\ell} - \cos \phi_s - (\phi_{n,\ell} + \pi + \phi_s)\sin \phi_{n,\ell})]^{1/2}}{nk} \\ & + \frac{\ell}{n} V(t) \end{aligned} \quad (91)$$

obtained from the general formulas (53) and (57), the green lines the correction due to the nonresonant waves, Eq. (89), and the yellow lines the corrected separatrices. Again, the agreement with the exact phase portraits is excellent.

## C. Interference effects

### 1. Derivation

A close look at Fig. 11 reveals small regions of phase stability centered at “strange” velocities, such as  $\frac{3}{2}V_0$  or  $2V_0$ . These phase-stable areas cannot arise from single-wave interactions, since, as we saw above, single waves travel at phase velocities  $\frac{\ell}{n}V_0$  with  $\ell$  and  $n$  odd. Here we will show that the phase-stable areas occurring at even-fraction multiples of  $V_0$  actually arise from the interference of two waves with  $n$  and  $\ell$  odd.

We reach this conclusion in *four steps*, outlined below for the case of guiding. *First*, we transform the equation of motion of a molecule at a position  $z$  subject to two arbitrary waves  $(+, n, \ell)$  and  $(+, r, s)$

$$\ddot{z} = A_{n,\ell} \sin(nkz - \ell \omega t) + A_{r,s} \sin(rkz - s \omega t) \quad (92)$$

cf. Eq. (35), to a frame moving with velocity

$$V_g = \frac{\ell + s}{n + r} V_0, \quad (93)$$

where the two waves act on the molecule with the same frequency

$$\omega_g = \frac{ns - \ell r}{n + r} \omega. \quad (94)$$

Note that  $\omega_g$  is a fast oscillation. The molecule's position in such a frame is

$$z_g = z - V_g t. \quad (95)$$

The transformed equation of motion thus becomes

$$\ddot{z}_g = A_{n,\ell} \sin(nkz_g + \omega_g t) + A_{r,s} \sin(rkz_g - \omega_g t), \quad (96)$$

where we made use of the equality  $\ddot{z} = \ddot{z}_g$ .

*Second*, we integrate Eq. (96) under the condition that the spatial phase  $kz_g$  remain constant with respect to the temporal phase  $\omega_g t$ ; this is consistent with our aim to find stable, slowly oscillating solutions. For the constant spatial phase we take the value  $nkz_g(t')$  the spatial phase acquires at an arbitrary time,  $t'$ . Thus we obtain

$$\begin{aligned} \dot{z}_g(t) &= -\frac{A_{n,\ell}}{\omega_g} \cos[nkz_g(t') + \omega_g t] + \frac{A_{r,s}}{\omega_g} \cos[rkz_g(t') - \omega_g t] \\ &\quad + C_1, \end{aligned} \quad (97)$$

where  $C_1$  is an integration constant, which can be evaluated by integrating both sides of Eq. (97) over a fast oscillation period,  $\tau_g \equiv \frac{2\pi}{\omega_g}$ . This yields

$$\frac{1}{\tau_g} \int_{t' - \tau_g/2}^{t' + \tau_g/2} \dot{z}_g(t) dt \equiv \bar{z}_g(t') = \dot{\bar{z}}_g(t') = C_1. \quad (98)$$

Now integrating Eq. (97) for  $nkz_g(t')$  constant yields

$$\begin{aligned} z_g(t) &= -\frac{A_{n,\ell}}{\omega_g^2} \sin[nkz_g(t') + \omega_g t] - \frac{A_{r,s}}{\omega_g^2} \sin[rkz_g(t') - \omega_g t] \\ &\quad + \dot{\bar{z}}_g(t')(t - t') + C_2, \end{aligned} \quad (99)$$

where we made use of Eq. (98). Here  $C_2$  is another integration constant, which can be evaluated by integrating Eq. (99) over a fast-oscillation period  $\tau_g$

$$\frac{1}{\tau_g} \int_{t' - \tau_g/2}^{t' + \tau_g/2} z_g(t) dt \equiv \bar{z}_g(t') = C_2. \quad (100)$$

Note that Eqs. (97) and (99) are valid at time  $t \approx t'$ . In particular, for  $t = t'$  Eq. (99) yields

$$\begin{aligned} z_g(t') &= -\frac{A_{n,\ell}}{\omega_g^2} \sin[nkz_g(t') + \omega_g t'] - \frac{A_{r,s}}{\omega_g^2} \sin[rkz_g(t') - \omega_g t'] \\ &\quad + \bar{z}_g(t'). \end{aligned} \quad (101)$$

Since the time  $t'$  was chosen arbitrarily, Eq. (101) holds at *all times*, which makes  $t'$  into a *time variable*; we will denote it by  $t$  again ( $t' \rightarrow t$ ). Furthermore, we will solve Eq. (101) iteratively. The inequalities  $A_{n,\ell}/\omega_g^2 \ll 1$

and  $A_{r,s}/\omega_g^2 \ll 1$  (cf. Sec. IV H) along with Eq. (101) imply that

$$z_g(t) \approx \bar{z}_g(t) \quad (102)$$

from which it follows that already the first iteration (i.e.,  $z_g(t) \rightarrow \bar{z}_g(t)$ , on the right-hand side) generates an accurate solution

$$\begin{aligned} z_g(t) &= -\frac{A_{n,\ell}}{\omega_g^2} \sin[nk\bar{z}_g(t) + \omega_g t] - \frac{A_{r,s}}{\omega_g^2} \sin[rk\bar{z}_g(t) - \omega_g t] \\ &\quad + \bar{z}_g(t) = a + b + \bar{z}_g, \end{aligned} \quad (103)$$

where the quantities  $a$  and  $b$  are shorthands for the first and second term, respectively.

*Third*, we insert Eq. (103) into the equation of motion (96) and invoke the following trigonometric approximations:

$$\begin{aligned} \sin[nk(a + b)] &\approx nk(a + b) \quad \sin[rk(a + b)] \approx rk(a + b) \\ \cos[nk(a + b)] &\approx 1 \quad \cos[rk(a + b)] \approx 1. \end{aligned} \quad (104)$$

As a result, we obtain the equation of motion in the form

$$\begin{aligned} \ddot{z}_g &\approx nkA_{n,\ell}(a + b)\cos(nk\bar{z}_g + \omega_g t) + rkA_{r,s}(a + b)\cos(rk\bar{z}_g \\ &\quad - \omega_g t) + A_{n,\ell}\sin(nk\bar{z}_g + \omega_g t) + A_{r,s}\sin(rk\bar{z}_g - \omega_g t) \\ &= [1 - \omega_g^{-2}[nkA_{n,\ell}\cos(nk\bar{z}_g + \omega_g t) + rkA_{r,s}\cos(rk\bar{z}_g \\ &\quad - \omega_g t)]] \times [A_{n,\ell}\sin(nk\bar{z}_g + \omega_g t) + A_{r,s}\sin(rk\bar{z}_g - \omega_g t)]. \end{aligned} \quad (105)$$

Taking an average of Eq. (105) over the fast-oscillation period  $\tau_g$  yields

$$\begin{aligned} \frac{1}{\tau_g} \int_{t - \tau_g/2}^{t + \tau_g/2} \ddot{z}_g(t) dt' &\equiv \bar{\ddot{z}}_g(t) = \ddot{\bar{z}}_g(t) \\ &= -\frac{1}{2\omega_g^2} A_{n,\ell} A_{r,s} (n+r) k \sin[(n+r)k\bar{z}_g]. \end{aligned} \quad (106)$$

Equation (106) is a second-order differential equation for  $\bar{z}_g$  which reveals that a molecule that has a coordinate  $z_g \approx \bar{z}_g$  with respect to a synchronous molecule traveling at a velocity  $V_g$  is subject to a sine-shaped restoring force which leads to slow stabilizing oscillations. This comes about in exactly the same manner as in the case of a single-wave interaction.

*Fourth*, we realize that the waves  $(+, n, \ell)$  and  $(+, r, s)$  act jointly as a single wave  $(+, n+r, \ell+s)$ . As this wave moves at the phase velocity  $V_g = \frac{\ell+s}{n+r} V_0$ , cf. Eq. (93), we can ascribe it a phase

$$\phi_{n+r, \ell+s} \equiv (n+r)kz - (\ell+s)\omega t. \quad (107)$$

Plugging Eqs. (93) and (95) into Eq. (107) then gives

$$\phi_{n+r, \ell+s} = (n+r)kz_g \approx (n+r)k\bar{z}_g, \quad (108)$$

which implies

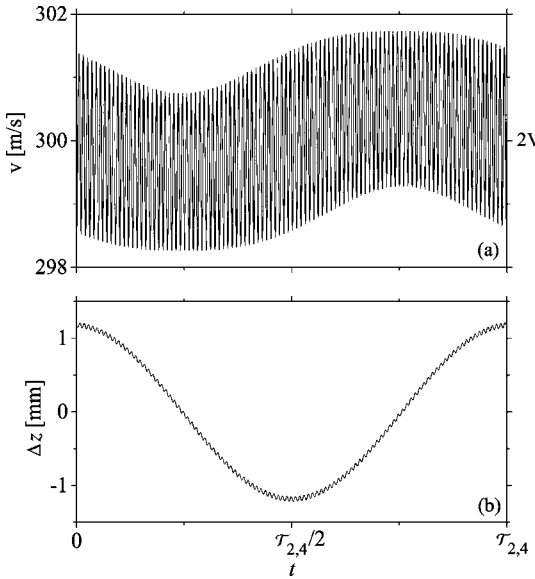


FIG. 14. Interference dynamics of a nonsynchronous molecule interacting with the (1, 1) wave and the (1, 3) wave which jointly create phase stability at  $2V_0$ . The dynamics was obtained by numerically integrating the equation of motion (92) for a molecule interacting with the two waves, with the initial condition  $v(0)=2V_0$ . Both the longitudinal velocity,  $v(t)$ , panel (a), and the relative position,  $\Delta z=z(t)-2V_0t$ , panel (b), exhibit slow oscillations superposed by fast oscillations. The two interfering waves (1, 1) and (1, 3) act jointly as a single (2, 4) wave, giving rise to slow oscillations of period  $T_{2,4}$ . Note the similarity with Fig. 9.

$$\ddot{\phi}_{n+r,\ell+s} \approx (n+r)k\ddot{z}. \quad (109)$$

Substitution from Eqs. (108) and (109) into Eq. (106) yields the final result

$$\begin{aligned} \ddot{\phi}_{n+r,\ell+s} &= -\frac{1}{2\omega_g^2}A_{n,\ell}A_{r,s}(n+r)^2k^2 \sin \phi_{n+r,\ell+s} \\ &= A_{n+r,\ell+s}(n+r)k \sin \phi_{n+r,\ell+s} \\ &= \alpha_{n+r,\ell+s} \sin \phi_{n+r,\ell+s}, \end{aligned} \quad (110)$$

where we set

TABLE I. A list of the properties of typical two-wave interference effects.

Interfering waves	(1,1),(1,3)	(1,1),(3,1)	(1,1),(5,7)	(3,7),(1,3)
$V_g$	$\frac{4}{2}V_0=2V_0$	$\frac{2}{4}V_0=\frac{1}{2}V_0$	$\frac{8}{6}V_0=\frac{4}{3}V_0$	$\frac{10}{4}V_0=\frac{5}{2}V_0$
$n+r$	2	4	6	4
$\omega_g$	$\omega$	$\omega/2$	$\omega/3$	$\omega/2$
$A_{n+r,\ell+s}$	$-\frac{4k^3W_1^2}{3\pi^2M^2\omega^2}$	$\frac{96k^3W_1W_3}{\pi^2M^2\omega^2}$	$-\frac{540k^3W_1W_5}{7\pi^2M^2\omega^2}$	$\frac{64W_1W_3}{7\pi^2M^2\omega^2}$

$$A_{n+r,\ell+s} \equiv -\frac{1}{2\omega_g^2}A_{n,\ell}A_{r,s}(n+r)k \quad (111)$$

and

$$\alpha_{n+r,\ell+s} \equiv A_{n+r,\ell+s}(n+r)k. \quad (112)$$

Equation (110) is of the same form as Eq. (43) for a single-wave interaction (in the case of guiding, with  $\sin\phi_s=0$ ). Therefore, all the results (for guiding) obtained from Eq. (43) are equally valid for the interference dynamics.

Figure 14 illustrates the interference dynamics of a molecule interacting with the (1, 1) and (1, 3) waves which propagate at phase velocities  $V_0$  and  $3V_0$ , respectively. The dynamics was obtained by numerical integration of Eq. (92), with the initial condition set such that  $v(0)=\frac{\ell+s}{n+r}V_0=2V_0$ . Note the similarity between Figs. 9 and 14. The former pertains to a nonsynchronous molecule interacting resonantly with the (3, 5) wave and nonresonantly with the (1, 1) wave. As a result, the molecule's velocity slowly oscillates about  $\frac{5}{3}V_0$ , with superposed fast oscillation due to the perturbation by the (1, 1) perturbing wave. Figure 14 shows a similar dynamics, but now the slow, stable velocity oscillation is centered around  $\frac{1+3}{1+1}V_0$ . Hence the (1, 1) and (1, 3) waves act individually as perturbing waves, but act jointly as a single stabilizing (2, 4) wave propagating at  $2V_0$ .

We note that the frequency and amplitude of the fast oscillations are correctly predicted by Eqs. (97) and (103).

## 2. Comparison with the exact phase portraits

Equipped with Eq. (110), we can now return to Fig. 11 and check whether the strange features occurring at even-fraction multiples of the fundamental velocity can indeed be explained by our analytic model of the Stark accelerator/decelerator.

First, we observe that the phase-stable areas are found at the velocities  $\frac{2}{4}V_0$ ,  $\frac{6}{4}V_0$ , and  $\frac{4}{2}V_0$ . Zooming in would reveal many more phase-stable areas, e.g., at  $\frac{10}{4}V_0$  or  $\frac{8}{6}V_0$ . The stability at all these velocities follows directly from Eqs. (93) and (110). Table I lists pairs of waves that give rise to a given phase-stable area due to interferences. Thus we see that, for instance, the stability at  $\frac{4}{2}V_0$  results from the interference of the (1, 1) and (1, 3) waves, and at  $\frac{2}{4}V_0$  from the interference of the (1, 1) and (3, 1) waves. Next, we observe that the phase-stable area at  $\frac{4}{2}V_0$  exhibits two fishes, whereas phase stability at  $\frac{2}{4}V_0$  exhibits four. Also this is in full agreement

with our treatment, and follows immediately from the  $(n+r)$  factor in the argument of the sine in Eq. (110). The sign of the prefactor  $\alpha_{n+r,\ell+s}$  explains correctly whether the interference effect exhibits a node or an antinode at  $z=0$ . Last but not least, we can evaluate the slow-oscillation frequency in the harmonic limit, cf. Eq. (63), from

$$\Omega = |\alpha_{n+r,\ell+s}|^{1/2} = (r+n)k \left| \frac{A_{n,\ell} A_{r,s}}{2\omega_g^2} \right|^{1/2} \equiv \Omega_{n+r,\ell+s}, \quad (113)$$

where the absolute value accommodates the cases of negative  $A_{n,\ell}$ ,  $A_{r,s}$ , or  $\omega_g$ .

Let us zoom in Fig. 11 on the phase-stable area occurring at  $2V_0$ , and use it as a testing ground for the accuracy of our treatment of the interference effects. A magnification of this phase-stable area is displayed in Fig. 15(a). The white curve shows the separatrix obtained from Eqs. (86) and (107) for the resonant  $(+, n+r, \ell+s) = (+, 2, 4)$  wave. We see that it correctly renders the size of the separatrix but not quite its shape. As in the case of single-wave dynamics, in order to obtain a full agreement between our theory and the exact result we have to take into account the influence of the perturbing waves. This influence can be taken into account in exactly the same way as before, i.e., by means of Eq. (89). We have to substitute into it  $n+r=2$  for  $n$  and  $\ell+s=4$  for  $\ell$ , which gives

$$\begin{aligned} \tilde{v}_{2,4}(z, t=0) &\approx \sum_{p \text{ odd}} \frac{2}{(2p-4)\omega} A_{1,p} \cos(kz) \\ &+ \sum_{p \text{ odd}} \frac{2}{(2p+4)\omega} A_{1,p} \cos(kz) - \frac{2}{8\omega} A_2 \cos(2kz) \\ &= \sum_{p \text{ odd}} \left( \frac{1}{(p-2)p} + \frac{1}{(p+2)p} \right) \frac{A_{1,1}}{\omega} \cos(kz) \\ &- \frac{A_2}{4\omega} \cos(2kz) = -\frac{A_2}{4\omega} \cos(2kz). \end{aligned} \quad (114)$$

We see that in this particular case, the sum over  $p$  vanishes and so the correction given by Eq. (114) takes quite a simple form. The correction is shown by the green curve in Fig. 15(a). The yellow curve is a sum of the white and green curves, and is seen to agree perfectly with the exact separatrix. We thus arrive at the conclusion that our analytic model accounts perfectly well for the observed phase stability at even-fraction multiples of the fundamental velocity, in terms of interferences of waves with  $n, \ell$  odd.

Above, we treated the dynamics due to two interfering waves. In particular, we showed that the  $(+, 1, 1)$  and the  $(+, 1, 3)$  waves jointly create phase stability at  $2V_0$ . But these are not the only waves that create stability at this velocity! An interference wave, just as a single wave, is always accompanied by fellow-traveler waves. For example, the  $(-, 1, 1)$  and  $(+, 1, 5)$  waves also create phase stability at  $2V_0$ , as do the  $(-, 1, 3)$  and the  $(+, 1, 7)$  waves, etc.

Taking into account all combinations of the  $(\pm, 1, \ell)$  waves that generate phase stability at  $2V_0$ , we obtain for the total  $\alpha_{2,4}$  coefficient

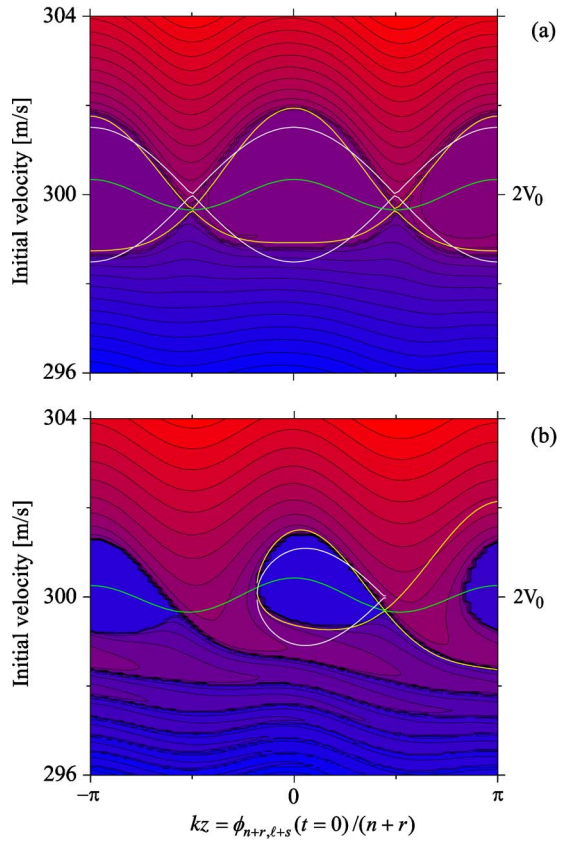


FIG. 15. (Color online) Detailed view of the phase stable area around  $2V_0$  for the case of guiding (with  $\phi_s=0^\circ$ ), panel (a), and of deceleration (with  $\phi_s=20^\circ$ ), panel (b). The contours pertain to average velocities of OH molecules plotted as a function of their initial velocity  $v$  and initial spatial phase  $kz$ . The full-fledged numerical calculations are compared with the analytic result for the case of the interference of the  $(1, 1)$  wave with the  $(1, 3)$  wave, which give jointly rise to a  $(2, 4)$  wave. The white curves show the separatrices (at  $t=0$ ) obtained from Eq. (53) for  $n \rightarrow n+r$  and  $\ell \rightarrow \ell+s$ , and with  $\phi_{n+r,\ell+s}$  and  $\alpha_{n+r,\ell+s}$  as given by Eqs. (107) and (112). The green curves were obtained from Eq. (114) and comprise the perturbations due to all nonresonant waves. The yellow curves combine the two and are seen to be in excellent agreement with the full-fledged numerical calculation. The temporal phase and switching sequence used for deceleration, panel (b), is given, respectively, by Eqs. (121) and (122). We note that the  $A_2$  coefficient is negative for the case of low-field seekers, considered in this calculation.

$$\alpha_{2,4} = -\frac{8k^4 W_1^2}{\pi^2 M^2 \omega^2} \left( \frac{1}{3} - \sum_{i=3,5,\dots}^{\infty} \frac{1}{i^2(i-2)(i+2)} \right) = -\frac{k^4 W_1^2}{4M^2 \omega^2}, \quad (115)$$

where we note that Eq. (115) is in complete agreement with Eq. 24 of Ref. [16]. The combined effect of the fellow-traveler waves is small. In total, they give rise to a correction of about 8% to the value of  $\alpha_{2,4}$  obtained by considering the  $(+, 1, 1)$  and  $(+, 1, 3)$  waves only. This results in a correction of 4% for the corresponding separatrix. Therefore, in evaluating the phase-stable areas around  $2V_0$ , we could rely solely on the interference wave arising from the combination of the  $(+, 1, 1)$  and  $(+, 1, 3)$  waves.

The same discussion can be applied to phase stability at  $\frac{1}{2}V_0$ , which is not due just to the  $(+, 1, 1)$  and  $(+, 3, 1)$  waves, but also to the  $(+, 1, 3)$  and  $(-, 3, 1)$  waves, the  $(-, 1, 1)$  and  $(+, 3, 3)$  waves, etc. Taking into account all combinations of the  $(\pm, 1, \ell)$  and  $(\pm, 3, \ell)$  waves that generate phase stability at  $\frac{1}{2}V_0$ , we obtain for the total  $\alpha_{4,2}$  coefficient

$$\alpha_{4,2} = \frac{96k^4W_1W_3}{\pi^2M^2\omega^2} \left[ 4 - \sum_{i=1,3,\dots}^{\infty} \left( \frac{1}{(i+1/2)^2i(i+2)} + \frac{1}{(i+3/2)^2i(i+2)} \right) \right] = \frac{16k^4W_1W_3}{M^2\omega^2} \left( 4 - \frac{16}{3\pi} \right), \quad (116)$$

which is in full agreement with Eq. 26 of Ref. [16]. Again, the correction due to the fellow-traveler waves has no significant effect on the size of the separatrix as evaluated from the combination of the  $(+, 1, 1)$  and  $(+, 3, 1)$  waves alone.

### 3. Accelerating or decelerating on an interference

Accelerating or decelerating on an interference wave is somewhat trickier than it is on a single wave. The main reason is that the  $A_{n+r,\ell+s}$  coefficient, Eq. (111), which depends on  $\omega$ , becomes itself time dependent through the time dependence of  $\omega=\omega(t)$ . This needs to be taken into account when re-deriving expressions for  $v_s(t)$  and  $\omega(t)$  from the condition of a constant synchronous phase with respect to the  $(n+r, \ell+s)$  wave.

First we realize that the acceleration imparted to the synchronous molecule by the interference wave is given by

$$a_s(t) = A_{n+r,\ell+s}(t) \sin \phi_s = -\frac{(n+r)^3}{2(ns-\ell r)^2\omega^2(t)} kA_{n,\ell}A_{r,s} \sin \phi_s \\ = \frac{A_d}{\omega^2(t)}, \quad (117)$$

where we made use of Eqs. (23), (94), and (111) and so is seen to depend on time. This time dependence does not affect the derivation of the interference dynamics (Sec. V C) since  $\omega(t)$  does not change appreciably during a fast-oscillation period. Equation (117) can be integrated to yield the synchronous velocity, which must equal the phase velocity

$$v_s(t) = \frac{\ell+s}{n+r}V_0 + \int_0^t a_s(t') dt' = \frac{\ell+s}{n+r}V_0 + \int_0^t \frac{A_d}{\omega^2(t')} dt' \\ = V_{n+r,\ell+s}(t) \equiv \frac{\ell+s}{n+r} \frac{\omega(t)}{k}. \quad (118)$$

The time derivative of Eq. (118) can be recast into a differential equation for  $\omega(t)$

$$\dot{\omega}(t) = \frac{n+r}{\ell+s} \frac{kA_d}{\omega^2(t)}, \quad (119)$$

which can be easily solved by direct integration. With the initial condition  $\omega(0)=\omega_0$  we obtain

$$\omega(t) = \left[ \frac{3(n+r)kA_d}{\ell+s} t + \omega_0^3 \right]^{1/3}. \quad (120)$$

From Eq. (120), the temporal phase becomes

$$\theta(t) = \int_0^t \omega(t') dt' = \frac{\ell+s}{4(n+r)kA_d} \left[ \frac{3(n+r)kA_d}{\ell+s} t + \omega_0^3 \right]^{4/3} \\ - \frac{(\ell+s)\omega_0^4}{4(n+r)kA_d}, \quad (121)$$

which generates the switching sequence required for accelerating or decelerating on an interference wave

$$\theta(t) = q\pi \quad q = 0, 1, 2, \dots \quad (122)$$

The switching sequence obtained from Eq. (121) was used in a full-fledged calculation for the case of deceleration (at  $\phi_s=20^\circ$ ) to generate the phase portrait shown in Fig. 15(b). Also shown is the separatrix (white curve) obtained by substituting  $\alpha_{n+r,\ell+s}(t=0)$  into Eq. (53). We note that the value of  $\alpha_{n+r,\ell+s}(t)$  at  $t=0$  is minimal, and so determines the depth of the potential well that captures the molecules which, in turn, determines the area of phase stability (note that any increase of the well depth during deceleration is of no avail). Also shown are the perturbations by all the other waves (green curve) and the net separatrix (yellow curve). Again, an excellent agreement between the latter and the full-fledged calculation is found. Deceleration on an interference is of little practical interest, since the corresponding deceleration rates and phase-stable areas are puny.

### 4. Multiple interferences

Furthermore, it is quite easy to generalize the treatment of the interference effect to more than two waves. This can be done by treating the interference wave on the same footing as a single wave and letting it interfere with another single wave, in exactly the same way as the two single waves that gave rise to the interference. This results in tiny, so far unobserved effects.

## VI. CONCLUSIONS

Stark acceleration or deceleration is a phase-stable process that enables full control of the translational motion of quantum-state-selected polar molecules. The acceleration or deceleration process abounds in rich dynamics, which has been accurately captured by an analytic model presented in this paper. The model is based on a Fourier analysis of the time-varying inhomogeneous electric field produced by a Stark accelerator/decelerator, which reveals that the field consists of an infinite multitude of stationary and counter-propagating waves with well defined phase velocities. The ensuing physical picture set forth by the “wave model” is

that molecules injected into the accelerator/decelerator ride the waves.

In this paper, we tackled explicitly the interaction of the injected molecules with an arbitrary wave in the Fourier expansion, and obtained an analytic description of the acceleration or deceleration dynamics which is both intuitive and exact. We found that the dynamics is dominated by the interaction of the molecules with a single wave. This wave is distinguished from all the other waves by its phase velocity, which is such as to come close to the velocity of the molecules (resonant wave). We studied explicitly the effect of the nonresonant, perturbing waves on the resonant-wave dynamics and showed that it is heavily suppressed, with little consequence for phase stability. We also showed that two (or more) waves can interfere with one another and act jointly as a single wave that gives rise to a phase-stable motion of the molecules.

We compared the dynamics derived from the wave model with Monte Carlo trajectory simulations of the acceleration or deceleration dynamics, which in previous work had been found to be in perfect agreement with experiment. This comparison showed that every tiny detail of the observed rich

phase-space structures could be accounted for by invoking either single-wave dynamics, or perturbations by nonresonant waves, or interference dynamics.

The link between various regions of phase stability and experimental observations was studied earlier [16]. However, the wave model led us to reinterpret the first- and second-order resonances, identified in the previous work, in terms of single-wave and interference dynamics. We were able to extend the previous study and show that arbitrary overtone waves can be used for deceleration. This was subsequently corroborated by experiment [26].

Thus we conclude that the analytic wave model encompasses all the longitudinal dynamics that arises in a Stark accelerator/decelerator.

## ACKNOWLEDGMENTS

We thank our colleagues at the Fritz-Haber-Institut for helpful discussions, in particular Dr. Rick Bethlem (now also at the Vrije Universiteit Amsterdam), Joop Gilliamse, Dr. Bas van de Meerakker, and Dr. Nicolas Vanhaecke (now at Laboratoire Aimé Cotton).

- 
- [1] C. H. Townes and A. L. Schawlow, *Microwave Spectroscopy* (Dover, New York, 1975).
  - [2] G. Scoles, *Atomic and Molecular Beam Methods* (Oxford University Press, New York, 1988).
  - [3] H. Pauly, *Atom, Molecule, and Cluster Beams* (Springer, Berlin, 2000).
  - [4] H. L. Bethlem, G. Berden, and G. Meijer, Phys. Rev. Lett. **83**, 1558 (1999).
  - [5] H. L. Bethlem, A. J. A. van Roij, R. T. Jongma, and G. Meijer, Phys. Rev. Lett. **88**, 133003 (2002).
  - [6] F. M. H. Crompvoets, R. T. Jongma, H. L. Bethlem, A. J. A. van Roij, and G. Meijer, Phys. Rev. Lett. **89**, 093004 (2002).
  - [7] S. A. Schulz, H. L. Bethlem, J. van Veldhoven, J. Küpper, H. Conrad, and G. Meijer, Phys. Rev. Lett. **93**, 020406 (2004).
  - [8] H. L. Bethlem, G. Berden, F. M. H. Crompvoets, R. T. Jongma, A. J. A. van Roij, and G. Meijer, Nature (London) **406**, 491 (2000).
  - [9] J. van Veldhoven, H. L. Bethlem, and G. Meijer, Phys. Rev. Lett. **94**, 083001 (2005).
  - [10] F. M. H. Crompvoets, H. L. Bethlem, R. T. Jongma, and G. Meijer, Nature (London) **411**, 174 (2001).
  - [11] S. Humphries, *Principles of Charged Particle Acceleration* (Wiley, New York, 1986).
  - [12] H. L. Bethlem, G. Berden, A. J. A. van Roij, F. M. H. Crompvoets, and G. Meijer, Phys. Rev. Lett. **84**, 5744 (2000).
  - [13] H. L. Bethlem, F. M. H. Crompvoets, R. T. Jongma, S. Y. T. van de Meerakker, and G. Meijer, Phys. Rev. A **65**, 053416 (2002).
  - [14] H. L. Bethlem and G. Meijer, Int. Rev. Phys. Chem. **22**, 73 (2003).
  - [15] B. Friedrich, Eur. Phys. J. D **31**, 313 (2004).
  - [16] S. Y. T. van de Meerakker, N. Vanhaecke, H. L. Bethlem, and G. Meijer, Phys. Rev. A **71**, 053409 (2005).
  - [17] S. Y. T. van de Meerakker, N. Vanhaecke, H. L. Bethlem, and G. Meijer, Phys. Rev. A **73**, 023401 (2006).
  - [18] G. B. Arfken and H. J. Weber, *Mathematical Methods for Physicists* (Academic Press, New York, 1995).
  - [19] B. Friedrich and D. R. Herschbach, Comments At. Mol. Phys. **32**, 47 (1995).
  - [20] The Stark-energy Fourier coefficients  $W_i$  of Eq. (14) coincide with the Stark-energy Fourier coefficients  $a_i$  introduced in previous work, Ref. [14], i.e.,  $W_i = a_i$ .
  - [21] Formula (34) is identical with Eq. (15) of Ref. [14] for  $n=\ell=1$  where, in the notation used in that reference, it takes the form  $t(q)=\frac{mL}{2a_1 \sin \phi_0} \left( v(z=0) - \sqrt{v^2(z=0) - \frac{4qa_1}{m} \sin \phi_0} \right)$ . The old notation translates into the new one in the following way:  $a_1 \rightarrow W_1$ ;  $\phi_0 \rightarrow \phi_s$ ;  $L \rightarrow \frac{\lambda}{2}$ , so that  $k = \frac{2\pi}{\lambda} = \frac{\pi}{L}$ ;  $m \rightarrow M$ ;  $v(z=0) \rightarrow V_0$ .
  - [22] Formula (64) differs from Eq. (10) of Ref. [16] which, in the old notation, cf. end note [21], reads  $\sqrt{\frac{a_n \cos(n\phi_0)}{2\pi m s L^2}}$ , and so is seen to lack a factor of  $n^{1/2}$  in the numerator.
  - [23] V. Veksler, J. Phys. (USSR) **9**, 153 (1944).
  - [24] E. M. McMillan, Phys. Rev. **68**, 143 (1945).
  - [25] R. Campargue, editor, *Atomic and Molecular Beams* (Springer, Berlin, 2001).
  - [26] K. Gubbels, Master's thesis, University of Nijmegen, 2006.